

Geometric Blow-up for Folded Limit Cycle Manifolds in Three Time-Scale Systems

S. Jelbart*, S.-V. Kuntz*[†] & C. Kuehn*

August 3, 2022

Abstract

Geometric singular perturbation theory provides a powerful mathematical framework for the analysis of ‘stationary’ multiple time-scale systems which possess a *critical manifold*, i.e. a smooth manifold of steady states for the limiting fast subsystem, particularly when combined with a method of desingularization known as *blow-up*. The theory for ‘oscillatory’ multiple time-scale systems which possess a limit cycle manifold instead of (or in addition to) a critical manifold is less developed, particularly in the non-normally hyperbolic regime. We show that the blow-up method can be applied to analyse the global oscillatory transition near a regular folded limit cycle manifold in a class of three time-scale systems with two small parameters. The systems considered behave like oscillatory systems as the smallest perturbation parameter tends to zero, and stationary systems as both perturbation parameters tend to zero. The additional time-scale structure is crucial for the applicability of the blow-up method, which cannot be applied directly to the two time-scale counterpart of the problem. Our methods allow us to describe the asymptotics and strong contractivity of all solutions which traverse a neighbourhood of the global singularity. Our results cover a range of different cases with respect to the relative time-scale of the angular dynamics and the parameter drift.

Keywords: Geometric singular perturbation theory, global fast-slow systems, three time-scale systems, geometric blow-up, limit cycle bifurcations

MSC2020: 34D15, 34E10, 34E13, 34E15, 34E20, 34C45, 34C27

1 Introduction

Many physical and applied systems featuring multiple time-scale dynamics can be mathematically modelled by singularly perturbed systems of ordinary differential equations in the standard form

$$\begin{aligned}x' &= f(x, y, \varepsilon), \\y' &= \varepsilon g(x, y, \varepsilon),\end{aligned}\tag{1}$$

where $x \in \mathbb{R}^m$, $y \in \mathbb{R}^n$, $(\cdot)' = d/dt$, $0 < \varepsilon \ll 1$ is a small perturbation parameter and the functions $f, g : \mathbb{R}^m \times \mathbb{R}^n \times [0, \varepsilon_0] \rightarrow \mathbb{R}^m \times \mathbb{R}^n$ are at least C^1 -smooth. If the limiting system obtained from (1) when $\varepsilon \rightarrow 0$ possesses a *critical manifold*, i.e. if the set of equilibria $S = \{(x, y) : f(x, y, 0) = 0\}$ forms an n -dimensional submanifold of the phase space $\mathbb{R}^m \times \mathbb{R}^n$, then system (1) can be analysed using a mathematical framework known as *geometric singular perturbation theory (GSPT)* [16, 26, 40, 57]. Typical GSPT analyses consist of two parts, depending on whether S is *normally hyperbolic*, i.e. depending on whether the linearisation with respect to the fast variables $D_x f|_S$ when $\varepsilon = 0$ is hyperbolic.

The local dynamics near normally hyperbolic submanifolds of S can be accurately described using *Fenichel-Tikhonov theory* [16, 55] (see also [26, 40, 57, 58]), which ensures that solutions are well approximated by regular perturbations of singular trajectories constructed as concatenations of trajectory segments from the distinct limiting problems which arise when $\varepsilon \rightarrow 0$ in system (1) on the fast and slow time-scales t and $\tau = \varepsilon t$, respectively. However, Fenichel-Tikhonov theory breaks down in the non-normally hyperbolic regime. The dynamics near non-normally hyperbolic points or submanifolds of S ,

*Department of Mathematics, The Technical University of Munich. Garching Bavaria, 85748, Germany.

[†]Corresponding author. Email: saraviola.kuntz@ma.tum.de

which generically correspond to bifurcations in the layer problem $(1)|_{\varepsilon=0}$, can be studied using various techniques. A particularly powerful approach is the so-called *blow-up method*, which was pioneered for fast-slow systems in [14] and later in [37, 38, 39]. In these works and many others (see [24] for a recent survey), the authors showed that the loss of hyperbolicity at a non-normally hyperbolic point or submanifold Q can often be ‘resolved’ after lifting the problem to a higher dimensional space in which Q is blown-up to a higher dimensional manifold \mathcal{Q} . Following a suitable *desingularization*, which amounts to a singular transformation of time, a non-trivial vector field with improved hyperbolicity properties can be identified on \mathcal{Q} . This allows one to study the dynamics in the non-normally hyperbolic regime using classical dynamical systems methods like regular perturbation and center manifold theory. We refer to [30, 31, 32, 34, 37, 38, 39, 42, 53, 54] for seminal works in both applied and theoretical contexts, based on this combination of Fenichel-Tikhonov theory and the blow-up method.

The mathematical theory and methods described above are local in the sense that they apply specifically to fast-slow systems possessing an n -dimensional critical manifold S . A corresponding global theory in which the layer problem $(1)|_{\varepsilon=0}$ possesses a limit cycle manifold in place of (or in addition to) a critical manifold is less developed. Following [21], we shall refer to the former class as *stationary* fast-slow systems, and the latter class as *oscillatory* fast-slow systems. A program for the development of a global GSPT which is general enough to encompass oscillatory fast-slow systems was initiated by J. Guckenheimer in 1996 [19], however a number of key analytical and methodological obstacles to its development remain.

One such obstacle concerns the development of Fenichel-Tikhonov theory for oscillatory fast-slow systems. A number of authors have made important contributions in this direction. Anosova showed that normally hyperbolic limit cycle manifolds in oscillatory fast-slow systems of the form (1) persist as $O(\varepsilon)$ -close locally invariant manifolds for the perturbed system [1, 2], similarly to the persistence of a normally hyperbolic critical manifold in Fenichel-Tikhonov theory. For oscillatory fast-slow systems with one slow variable, the persistence and contractivity properties of the center-stable/unstable manifolds have been described in detail in [25] using properties of the Poincaré map and a discrete GSPT framework developed therein. This study also yielded an asymptotic formula for the slow drift along the manifold, which agrees with the formula predicted by classical averaging theory [50]. Furthermore, these works are consistent with the findings of embedding-based approaches which suggest that oscillatory fast-slow systems can to a certain extent be ‘reduced’ to approximating stationary fast-slow systems in the normally hyperbolic regime; see e.g. [21, 22].

Global theory for oscillatory fast-slow systems in the non-normally hyperbolic regime is less developed, despite the ubiquity of fast-slow extensions of global bifurcations in applications, for example in biochemical models exhibiting *bursting* [7, 15, 20, 51]. A notable exception has been the rigorous topological classification of so-called *torus canards* in [56], which occur near folded cycle bifurcations in the layer problem in oscillatory fast-slow systems [56]. See e.g. [5, 6, 12, 33, 52] for more (predominantly numerical) important work on torus canards. The results in [56] were obtained using averaging theory, Floquet theory and (stationary) GSPT. Indirect contributions to the non-normally hyperbolic theory for oscillatory fast-slow systems have also been made via the study of non-normally hyperbolic singularities in fast-slow maps, since these can be used to infer dynamical properties of corresponding limit cycle bifurcations (or fast-slow extensions thereof) in one greater dimension. The slow passage through a flip/period-doubling bifurcation (and even through an entire period-doubling cascade) was treated in [3, 4], and further results on the slow passage through discrete transcritical, pitchfork and Neimark-Sacker/torus type bifurcations have been derived using non-standard analysis; we refer to the review paper [17] and the references therein.

In general, the development of mathematical methods for handling non-hyperbolic dynamics in oscillatory fast-slow systems is complicated by the fact that local techniques like the blow-up method rely upon near-equilibrium properties possessed by stationary but not oscillatory fast-slow systems. The desingularization step in blow-up analyses, for example, relies upon a formal division of the blown-up vector field by zero. This step is crucial for obtaining a desingularized vector field with improved hyperbolicity properties, but it is only well-defined if the original (blown-up) vector field is in equilibrium wherever it is formally divided by zero. For oscillatory fast-slow systems of the form (1), a ‘typical’ non-normally hyperbolic cycle has non-equilibrium dynamics, so it cannot be desingularized and the blow-up method does not apply.

The aim of this work is to show that stationary methods (in particular the blow-up method) which may not apply for oscillatory fast-slow systems, may be applicable in the study of oscillatory multiple time-scale systems with at least three distinct time-scales. Specifically, we consider systems of the form

$$\begin{aligned} r' &= f(r, \theta, y, \varepsilon_1, \varepsilon_2), \\ \theta' &= \varepsilon_1 g(r, \theta, y, \varepsilon_1, \varepsilon_2), \\ y' &= \varepsilon_2 h(r, \theta, y, \varepsilon_1, \varepsilon_2), \end{aligned} \tag{2}$$

where $(r, \theta, y) \in \mathbb{R}_{\geq 0} \times \mathbb{R}/\mathbb{Z} \times \mathbb{R}$ are cylindrical coordinates, $0 < \varepsilon_1, \varepsilon_2 \ll 1$ are singular perturbation parameters, and $f, g, h : \mathbb{R}_{\geq 0} \times \mathbb{R}/\mathbb{Z} \times \mathbb{R} \times [0, \varepsilon_{1,0}] \times [0, \varepsilon_{2,0}] \rightarrow \mathbb{R}_{\geq 0} \times \mathbb{R}/\mathbb{Z} \times \mathbb{R}$ are sufficiently smooth for our purposes (C^3 -smoothness will suffice). Depending upon the relative magnitude of ε_1 and ε_2 , system (2) has either two or three distinct time-scales. Although we present results on a range of different cases, we are primarily interested in the case

$$0 < \varepsilon_2 \ll \varepsilon_1 \ll 1, \tag{3}$$

which defines a class of three time-scale systems that are in a certain sense ‘in between’ the classes of stationary and oscillatory fast-slow systems described above. Heuristically, this is because under suitable assumptions (to be outlined in detail in Section 2), system (2) is an oscillatory fast-slow system with respect to the limit $\varepsilon_1 > 0$, $\varepsilon_2 \rightarrow 0$, and a stationary fast-slow system with respect to the double singular limit $(\varepsilon_1, \varepsilon_2) \rightarrow (0, 0)$ [41]. It is worthy to note that multiple time-scale systems with more than two time-scales appear frequently in applications. The long term dynamics of a forced VdP oscillator with three time-scales was studied as early as 1947 in [10]. A theoretical basis for normally hyperbolic theory for stationary multiple time-scale systems with three or more time-scales has appeared more recently in e.g. [8, 9, 35, 45]. Progress has also been made in the non-normally hyperbolic setting, particularly via the study of three time-scale applications and ‘prototypical systems’ inspired by applications; we refer to [11, 13, 23, 27, 28, 29, 36, 44, 47].

We present a detailed analysis of the ‘jump-type’ transition near a non-normally hyperbolic cycle of regular fold type using geometric blow-up. More precisely, we assume that the limiting system $(2)_{\varepsilon_1 > 0, \varepsilon_2 = 0}$ undergoes a codimension-1 folded cycle bifurcation under variation in y . This can be seen as the oscillatory analogue of the regular fold or jump point in stationary fast-slow systems, which has been studied using blow-up techniques in [37]; see also [46] for a detailed treatment using classical asymptotic methods. After deriving a suitable ‘normal form’ for the fast-slow fold of cycles in multiple time-scale systems of the form (2), we show that the blow-up method can be applied, even though a rigorous reduction to the stationary setting is not possible due to angular coupling in the higher order terms. The formal division by zero which is necessary to obtain a desingularized vector field with improved hyperbolicity properties is possible if the time-scale associated to the rotation is sufficiently slow relative to the fast radial dynamics, i.e. if ε_1 is sufficiently small. We also identify the fastest possible time-scale for the rotation (i.e. the scaling condition under which our methods apply), which can be quantified in terms of ε_2 , which measures the time-scale separation between the fast radial dynamics in r and slow parameter drift in y .

The blow-up analysis allows for the detailed characterisation of the transition map induced by the flow, including the asymptotic and contractivity properties of the transition undergone by solutions traversing the neighbourhood of the global singularity. In particular, under suitable assumptions the rotational coordinate is shown to decouple in the limiting (desingularized) system on the blow-up surface (a ‘torus of spheres’ $S^1 \times S^2$), allowing us to use pre-existing results from stationary fast-slow theory (particularly those in [37]) to study the leading order dynamics. The asymptotics for the parameter drift in y are shown to agree with the known results for the stationary regular fold point [37]. We also provide asymptotics for the angular coordinate θ as a function of the initial conditions and small parameters, and an asymptotic estimate for the number of rotations about the y -axis over the course of the transition. The results obtained are shown to depend on the relative magnitude of ε_1 and ε_2 , with the main qualitative difference pertaining to the asymptotic estimates for θ and the corresponding number of rotations. Although we are primarily motivated to understand the dynamics of systems with a time-scale structure induced by the scaling (3), we present results pertaining to all three possibilities for the relative speed of the angular and drift velocities, namely

(C1) $0 < \varepsilon_2 \ll \varepsilon_1 \ll 1$: Rotation is fast relative to the parameter drift;

(C2) $0 < \varepsilon_2 \sim \varepsilon_1 \ll 1$: Rotation and parameter drift occur on the same time-scale;

(C3) $0 < \varepsilon_1 \ll \varepsilon_2 \ll 1$: Rotation is slow relative to the parameter drift.

Due to decoupling of the angular dynamics in the leading order (i.e. in the desingularized system on $S^1 \times S^2$), all three cases can be treated simultaneously.

The manuscript is structured as follows. In Section 2 we introduce defining assumptions and present the normal form for which our main results are stated. The singular dynamics and geometry, which differ in each case (C1), (C2) and (C3), are presented in Section 2.1. The main results are presented and described in Section 3, and the blow-up analysis and proof of the main results are presented in Section 4. We conclude with a summary and outlook in Section 5.

2 Assumptions and setting

We consider C^k -smooth multiple time-scale systems in the general form (2), restated here for convenience:

$$\begin{aligned} r' &= f(r, \theta, y, \varepsilon_1, \varepsilon_2), \\ \theta' &= \varepsilon_1 g(r, \theta, y, \varepsilon_1, \varepsilon_2), \\ y' &= \varepsilon_2 h(r, \theta, y, \varepsilon_1, \varepsilon_2), \end{aligned} \tag{4}$$

where $k \geq 3$, $(\cdot)' = d/dt$, the variables are given in cylindrical coordinates $(r, \theta, y) \in \mathbb{R}_{\geq 0} \times \mathbb{R}/\mathbb{Z} \times \mathbb{R}$, and $\varepsilon_1, \varepsilon_2$ are singular perturbation parameters satisfying $0 < \varepsilon_1, \varepsilon_2 \ll 1$. System (4) evolves on either two or three time-scales, depending on whether the ratio $\varepsilon_1/\varepsilon_2$ is asymptotically large, constant or small. The setup and defining assumptions presented below are primarily motivated by the case $0 < \varepsilon_2 \ll \varepsilon_1 \ll 1$, for which system (4) in a certain sense ‘intermediate’ between stationary and oscillatory fast-slow systems. Since we also consider other possibilities, however, we leave the exact relation between ε_1 and ε_2 unspecified for now. It suffices to observe that the forward evolution of a generic initial condition is characterised by radial motion on the fast time-scale t , angular motion on a time-scale $\tau_{\varepsilon_1} = \varepsilon_1 t$, and vertical ‘parameter drift’ on a time-scale $\tau_{\varepsilon_2} = \varepsilon_2 t$.

In the following we impose a number of defining conditions in terms of the limiting oscillatory fast-slow system obtained in the singular limit $\varepsilon_1 > 0$, $\varepsilon_2 \rightarrow 0$, i.e. on

$$\begin{aligned} r' &= f(r, \theta, y, \varepsilon_1, 0), \\ \theta' &= \varepsilon_1 g(r, \theta, y, \varepsilon_1, 0), \\ y' &= 0. \end{aligned} \tag{5}$$

We remark that the singular limit $\varepsilon_1 > 0$, $\varepsilon_2 \rightarrow 0$ is only ‘natural’ if the rotation is fast relative to the parameter drift, i.e. if $\varepsilon_1/\varepsilon_2 \gg 1$.

Assumption 1. (Fast-slow oscillation for $\varepsilon_1 > 0$, $\varepsilon_2 \rightarrow 0$). *There exists a constant $\varepsilon_{1,0} > 0$ such that for all $\varepsilon_1 \in (0, \varepsilon_{1,0})$, system (5) has a two-dimensional manifold of regular limit cycles*

$$S_0 = \{(r, \theta, y) \in \mathbb{R}_{>0} \times \mathbb{R}/\mathbb{Z} \times \mathbb{R} : f(r, \theta, y, \varepsilon_1, 0) = 0\}.$$

In particular, there is a constant $v > 0$ such that S_0 contains the circular cycle $S_0^c = \{(v, \theta, 0) : \theta \in \mathbb{R}/\mathbb{Z}\}$.

The existence of a limit cycle manifold S_0 amounts to the assumption that system (4) is an oscillatory fast-slow system with respect to the (partial) singular limit $\varepsilon_1 > 0$, $\varepsilon_2 \rightarrow 0$. Note that Assumption 1 implies

$$f(v, \theta, 0, \varepsilon_1, 0) = 0, \quad g(v, \theta, 0, \varepsilon_1, 0) \neq 0,$$

for all $\theta \in \mathbb{R}/\mathbb{Z}$ and $\varepsilon_1 \in [0, \varepsilon_{1,0})$, where the latter follows from the assumption that S_0^c is a regular limit cycle. In what follows we assume that $g(v, \theta, 0, \varepsilon_1, 0) > 0$ without loss of generality.

Assumption 2. (S_0^c is a regular folded cycle). *The following defining conditions for a regular folded cycle are satisfied at S_0^c :*

(A1) The fast equation for r satisfies the fold condition

$$\frac{\partial f}{\partial r}(v, \theta, 0, \varepsilon_1, 0) = 0,$$

and the genericity conditions

$$\frac{\partial^2 f}{\partial r^2}(v, \theta, 0, \varepsilon_1, 0) \neq 0, \quad \frac{\partial f}{\partial y}(v, \theta, 0, \varepsilon_1, 0) \neq 0,$$

for all $\theta \in \mathbb{R}/\mathbb{Z}$ and $\varepsilon_1 \in [0, \varepsilon_{1,0})$.

(A2) The slow equation for y satisfies the regularity condition

$$h(v, \theta, 0, \varepsilon_1, 0) \neq 0,$$

for all $\theta \in \mathbb{R}/\mathbb{Z}$ and $\varepsilon_1 \in [0, \varepsilon_{1,0})$.

Assumption 2 ensures that system (4) has a regular folded cycle at $S_0^c \subset S_0$ when considered with respect to the limit $\varepsilon_1 > 0$, $\varepsilon_2 \rightarrow 0$. The defining conditions (A1) and (A2) are directly analogous to the defining conditions for the (stationary) regular fold point in [37]. The combination of signs taken by the various non-zero terms in (A1) and (A2) determines the orientation of the bifurcation. In the following we assume without loss of generality that

$$\frac{\partial^2 f}{\partial r^2}(v, \theta, 0, \varepsilon_1, 0) > 0, \quad \frac{\partial f}{\partial y}(v, \theta, 0, \varepsilon_1, 0) < 0, \quad h(v, \theta, 0, \varepsilon_1, 0) < 0, \quad (6)$$

which are consistent with a ‘jump-type’ orientation in forward time; see Figures 1 and 2. Based on Assumptions 1-2 and these sign conventions, it suffices to work with the local normal form provided in the following result.

Proposition 2.1. *Let Assumptions 1-2 be satisfied. Following a positive transformation of time, system (4) can be locally smoothly transformed into*

$$\begin{aligned} r' &= -y + r^2 + \varepsilon_1 a(\theta, \varepsilon_1)r + \mathcal{R}_r(r, \theta, y, \varepsilon_1, \varepsilon_2), \\ \theta' &= \varepsilon_1 b(\theta, \varepsilon_1), \\ y' &= \varepsilon_1 c(\theta, \varepsilon_1)y + \varepsilon_2(-1 + \mathcal{R}_y(r, \theta, y, \varepsilon_1, \varepsilon_2)), \end{aligned} \quad (7)$$

where (r, θ, y) are new cylindrical coordinates with a signed radius $r \in (-v\tilde{a}(\theta, \varepsilon_1), \infty)$, where $\tilde{a}(\theta, \varepsilon_1)$ is a continuous and uniformly positive function. The functions $a(\theta, \varepsilon_1)$, $b(\theta, \varepsilon_1)$, $c(\theta, \varepsilon_1)$ are smooth, $b(\theta, \varepsilon_1) > 0$ and

$$\mathcal{R}_r(r, \theta, y, \varepsilon_1, \varepsilon_2) = \mathcal{O}(r^3, y^2, ry, \varepsilon_2), \quad \mathcal{R}_y(r, \theta, y, \varepsilon_1, \varepsilon_2) = \mathcal{O}(r, y, \varepsilon_2).$$

Proof. Consider system (4) under Assumptions 1-2. We first divide the right-hand side by $g(r, y, \theta, \varepsilon_1, \varepsilon_2)$ (which is positive near $r = v$) by applying a positive transformation of time $d\tilde{t} = g(r, v, \theta, \varepsilon_1, \varepsilon_2)dt$, and move the cycle S_0^c to the ‘origin’ via the coordinate translation $\tilde{r} := r - v$. Taylor expanding the resulting equations about $\tilde{r} = y = \varepsilon_2 = 0$, we obtain

$$\begin{aligned} \tilde{r}' &= -f_1(\theta, \varepsilon_1)y + f_2(\theta, \varepsilon_1)\tilde{r}^2 + \mathcal{O}(\tilde{r}^3, y^2, \tilde{r}y, \varepsilon_2), \\ \theta' &= \varepsilon_1, \\ y' &= \varepsilon_2(-h_0(\theta, \varepsilon_1) + \mathcal{O}(\tilde{r}, y, \varepsilon_2)), \end{aligned} \quad (8)$$

where $f_1(\theta, \varepsilon_1)$, $f_2(\theta, \varepsilon_1)$ are smooth and positive (this follows from Assumption 2 and the sign conventions (6)), $h_0(\theta, \varepsilon_1) := h(v, \theta, 0, \varepsilon_1, 0) > 0$, and the dash notation denotes differentiation with respect to the new time \tilde{t} .

In order to obtain system (7) we look for a transformation of the form

$$\hat{r} = \tilde{a}(\theta, \varepsilon_1)\tilde{r}, \quad \hat{y} = \tilde{b}(\theta, \varepsilon_1)y, \quad d\hat{t} = \tilde{c}(\theta, \varepsilon_1)d\tilde{t},$$

where $\tilde{a}(\theta, \varepsilon_1)$, $\tilde{b}(\theta, \varepsilon_1)$ and $\tilde{c}(\theta, \varepsilon_1)$ satisfy

$$\frac{\tilde{a}(\theta, \varepsilon_1)}{\tilde{b}(\theta, \varepsilon_1)\tilde{c}(\theta, \varepsilon_1)}f_1(\theta, \varepsilon_1) = 1, \quad \frac{1}{\tilde{a}(\theta, \varepsilon_1)\tilde{c}(\theta, \varepsilon_1)}f_2(\theta, \varepsilon_1) = 1, \quad \frac{\tilde{b}(\theta, \varepsilon_1)}{\tilde{c}(\theta, \varepsilon_1)}h_0(\theta, \varepsilon_1) = 1.$$

Solving these constraints for \tilde{a} , \tilde{b} and \tilde{c} leads to the coordinate transformation

$$\hat{r} := \left(\frac{f_2(\theta, \varepsilon_1)^2}{f_1(\theta, \varepsilon_1)h_0(\theta, \varepsilon_1)} \right)^{1/3} \tilde{r}, \quad \hat{y} := \left(\frac{f_1(\theta, \varepsilon_1)f_2(\theta, \varepsilon_1)}{h_0(\theta, \varepsilon_1)^2} \right)^{1/3} y, \quad (9)$$

together with

$$d\hat{t} := (f_1(\theta, \varepsilon_1)f_2(\theta, \varepsilon_1)h_0(\theta, \varepsilon_1))^{1/3} dt. \quad (10)$$

Note that the domain for the new variable \hat{r} is

$$\hat{r} = \tilde{a}(\theta, \varepsilon_1)\tilde{r} = \tilde{a}(\theta, \varepsilon_1)(r - v) \in (-v\tilde{a}(\theta, \varepsilon_1), \infty),$$

as required. Applying (9) and (10) to system (8) leads to system (7) up to a change of notation $(r, y) \leftrightarrow (\hat{r}, \hat{y})$ (the coordinates (r, y) in (4) should not be confused with (r, y) in (7)), where

$$\begin{aligned} a(\theta, \varepsilon_1) &:= \frac{1}{3} \left(\frac{f_2(\theta, \varepsilon_1)^2}{f_1(\theta, \varepsilon_1)h_0(\theta, \varepsilon_1)} \right)^{-2/3} \frac{\partial}{\partial \theta} \left(\frac{f_2(\theta, \varepsilon_1)^2}{f_1(\theta, \varepsilon_1)h_0(\theta, \varepsilon_1)} \right), \\ b(\theta, \varepsilon_1) &:= (f_1(\theta, \varepsilon_1)f_2(\theta, \varepsilon_1)h_0(\theta, \varepsilon_1))^{-1/3}, \\ c(\theta, \varepsilon_1) &:= \frac{1}{3} \left(\frac{f_1(\theta, \varepsilon_1)f_2(\theta, \varepsilon_1)}{h_0(\theta, \varepsilon_1)^2} \right)^{-2/3} \frac{\partial}{\partial \theta} \left(\frac{f_1(\theta, \varepsilon_1)f_2(\theta, \varepsilon_1)}{h_0(\theta, \varepsilon_1)^2} \right)^{1/3}. \end{aligned}$$

Note that $b(\theta, \varepsilon_1) > 0$ as required, since $f_1(\theta, \varepsilon_1)$, $f_2(\theta, \varepsilon_1)$ and $h_0(\theta, \varepsilon_1)$ are positive. \square

System (7) is in 1-1 correspondence with the local normal form for the regular fold point in [39] if $\varepsilon_1 = 0$, i.e. if θ is fixed. For $\varepsilon_1 > 0$, however, the dependence on the angular variable appears via the functions $a(\theta, \varepsilon_1)$, $b(\theta, \varepsilon_1)$, $c(\theta, \varepsilon_1)$ and the higher order terms $\mathcal{R}_r(r, \theta, y, \varepsilon_1, \varepsilon_2)$ and $\mathcal{R}_y(r, \theta, y, \varepsilon_1, \varepsilon_2)$.

Remark 2.2. *In proof of Proposition 2.1 and in many of the proofs below we make use of transformations of time which are formulated in terms of differentials, e.g. $d\hat{t} = g(r, v, \theta, \varepsilon_1, \varepsilon_2)dt$. Strictly speaking, such an ‘transformation’ only defines \hat{t} as a unique function of t up to an additive constant. Since we are interested in the behaviour of solutions to autonomous ODEs, which are invariant under time translation, this additive constant can be set to zero without loss of generality.*

We impose one more assumption on system (7) for simplicity.

Assumption 3. (Angular coupling is higher order). We assume that

$$a(\theta, \varepsilon_1) \equiv 0, \quad b(\theta, \varepsilon_1) \equiv 1, \quad c(\theta, \varepsilon_1) \equiv 0,$$

such that system (7) only depends on θ via the higher order terms $\mathcal{R}_r(r, \theta, y, \varepsilon_1, \varepsilon_2)$, $\mathcal{R}_y(r, \theta, y, \varepsilon_1, \varepsilon_2)$.

Assumption 3 simplifies the analysis of later sections, but is not strictly necessary for our approach. We shall work exclusively with system (7) under Assumption 3 for the remainder of this manuscript, i.e. with the simplified normal form

$$\begin{aligned} r' &= -y + r^2 + \mathcal{R}_r(r, \theta, y, \varepsilon_1, \varepsilon_2), \\ \theta' &= \varepsilon_1, \\ y' &= \varepsilon_2(-1 + \mathcal{R}_y(r, \theta, y, \varepsilon_1, \varepsilon_2)), \end{aligned} \quad (11)$$

where we recall that r now defines a *signed* radial variable on $(-v\tilde{a}(\theta, \varepsilon_1), \infty)$, as in Proposition 2.1. Since we are primarily interested in the local dynamics near $r = 0$, it suffices to consider the dynamics in a domain with $r \in [-\tilde{v}, \infty)$, where \tilde{v} is a positive constant such that $\tilde{v} < v\tilde{a}(\theta, \varepsilon_1)$ for all $\theta \in \mathbb{R}/\mathbb{Z}$ and $\varepsilon_1 \in [0, \varepsilon_{1,0}]$.

Remark 2.3. *The methods and techniques applied below can be adapted to apply to the ‘full’ normal form in Proposition 2.1, i.e. without the additional simplification afforded by Assumption 3. We opt to focus on the simplified normal form (11) since our focus is on the applicability of certain methods in three time-scale systems (4), notably Fenichel-Tikhonov theory and the blow-up method. Since our primary focus is to provide a clear presentation of a method, the detailed treatment of the full normal form is left for future work.*

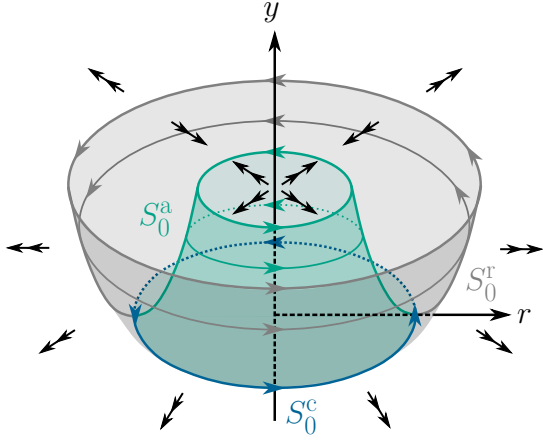


Figure 1: Singular geometry and dynamics in case (C1). Fast and slow dynamics are depicted (here and throughout) by double and single arrows respectively. The attracting and repelling normally hyperbolic submanifolds of the critical manifold S_0 , denoted by S_0^a and S_0^r , are shown in shaded turquoise and grey respectively. The non-normally hyperbolic folded cycle S_0^c is shown in blue. The reduced flow in case (C1) is periodic, i.e. y is a parameter and S_0 is foliated by limit cycles of period $\tau_{\varepsilon_1} = 1$.

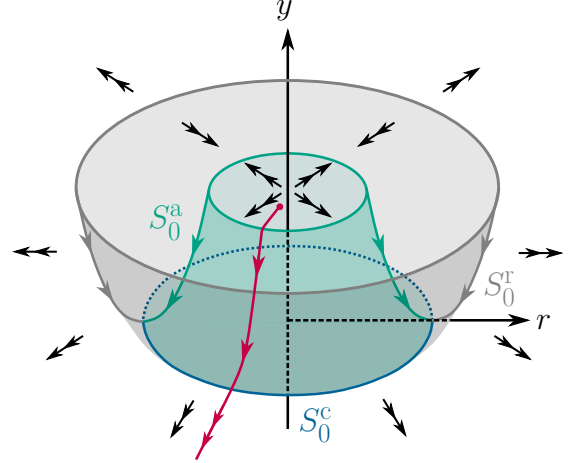


Figure 2: Singular geometry and dynamics in case (C3). The dynamics is distinguished from cases (C1) and (C2) by the reduced flow on S_0 . In this case, θ is a parameter and singular orbits (concatenations of solution segments of layer and reduced problem) are contained within constant angle planes $\{\theta = \text{const.}\}$. An example of such an orbit is sketched in red.

2.1 Geometry and dynamics in the singular limit

We turn now to the singular geometry and dynamics of the (simplified) normal form (11). Taking the double singular limit $(\varepsilon_1, \varepsilon_2) \rightarrow (0, 0)$ yields the *layer problem*

$$\begin{aligned} r' &= -y + r^2 + \mathcal{R}_r(r, \theta, y, 0, 0), \\ \theta' &= 0, \\ y' &= 0, \end{aligned} \tag{12}$$

which has a two-dimensional *critical manifold*

$$S_0 := \{(r, \theta, \varphi_0(r, \theta)) : r \in I_r, \theta \in \mathbb{R}/\mathbb{Z}\},$$

where $I_r := (-\tilde{r}_0, \tilde{r}_0)$ for a small but fixed $\tilde{r}_0 \in (0, \tilde{v}]$ and $y = \varphi_0(r, \theta) = r^2 + \mathcal{O}(r^3)$ solves the equation $-y + r^2 + \mathcal{R}_r(r, \theta, y, 0, 0) = 0$ locally via the implicit function theorem.

The stability of S_0 with respect to the fast radial dynamics is determined by the unique non-trivial (i.e. not identically zero) eigenvalue of the linearisation, namely

$$\lambda(r, \theta) = \left. \frac{\partial}{\partial r} (-y + r^2 + \mathcal{R}_r(r, \theta, y, 0, 0)) \right|_{S_0} = 2r + \mathcal{O}(r^2).$$

It follows that the critical manifold has the structure $S_0 = S_0^a \cup S_0^c \cup S_0^r$, where

$$S_0^a = \{(r, \theta, \varphi_0(r, \theta)) \in S_0 : r < 0\}, \quad S_0^r = \{(r, \theta, \varphi_0(r, \theta)) \in S_0 : r > 0\},$$

are normally hyperbolic and attracting/repelling, respectively. The circular set $S_0^c = \{(0, \theta, 0) \in S_0\}$, which corresponds to the regular folded cycle in Assumption 2, is non-normally hyperbolic. The situation is sketched in Figures 1 and 2.

The dynamics and geometry for the layer problem (12) do not depend upon the relative magnitude of ε_1 and ε_2 . The reduced dynamics on S_0 , however, are expected to differ significantly depending on the size of $\varepsilon_1/\varepsilon_2$. As noted already in Section 1, we consider three distinct possibilities:

(C1) Angular dynamics are fast relative to the parameter drift, i.e.

$$\frac{\varepsilon_1}{\varepsilon_2} \gg 1.$$

(C2) Angular dynamics occur on the same time-scale as the parameter drift, i.e. there is a constant $\sigma > 0$ such that

$$\frac{\varepsilon_1}{\varepsilon_2} = \sigma.$$

(C3) Angular dynamics are slow relative to the parameter drift, i.e.

$$\frac{\varepsilon_1}{\varepsilon_2} \ll 1.$$

A different reduced problem is obtained on S_0 in each case. We briefly consider each case in turn.

The reduced problem in case (C1)

In this case we rewrite system (11) on the slow time-scale $\tau_{\varepsilon_1} = \varepsilon_1 t$. This leads to

$$\begin{aligned} \varepsilon_1 \dot{r} &= -y + r^2 + \mathcal{R}_r(r, \theta, y, \varepsilon_1, \varepsilon_2), \\ \dot{\theta} &= 1, \\ \dot{y} &= \frac{\varepsilon_2}{\varepsilon_1}(-1 + \mathcal{R}_y(r, \theta, y, \varepsilon_1, \varepsilon_2)), \end{aligned} \tag{13}$$

where the dot denotes differentiation with respect to the slow time τ_{ε_1} . Since $\varepsilon_1/\varepsilon_2 \gg 1$, we obtain the reduced problem

$$\begin{aligned} 0 &= -y + r^2 + \mathcal{R}_r(r, \theta, y, 0, 0), \\ \dot{\theta} &= 1, \\ \dot{y} &= 0, \end{aligned} \tag{14}$$

in the double singular limit $(\varepsilon_1, \varepsilon_2) \rightarrow (0, 0)$. The slow variable y becomes a parameter in system (14), and S_0 is foliated by limit cycles of period $\tau_{\varepsilon_1} = 1$, i.e. $t = 1/\varepsilon_1$. This case is sketched in Figure 1.

The reduced problem in case (C2)

To obtain the reduced problem in case (C2) we may write system (11) on either time-scale τ_{ε_1} or τ_{ε_2} , which are related via $\tau_{\varepsilon_1} = \sigma \tau_{\varepsilon_2}$. Writing the system on the τ_{ε_2} time-scale leads to

$$\begin{aligned} \varepsilon_2 \dot{r} &= -y + r^2 + \mathcal{R}_r(r, \theta, y, \varepsilon_1, \varepsilon_2), \\ \dot{\theta} &= \frac{\varepsilon_1}{\varepsilon_2}, \\ \dot{y} &= -1 + \mathcal{R}_y(r, \theta, y, \varepsilon_1, \varepsilon_2), \end{aligned} \tag{15}$$

where this time, the dot denotes differentiation with respect to the slow time τ_{ε_2} . Taking the double singular limit and using the fact that $\varepsilon_1/\varepsilon_2 = \sigma$ leads to the reduced problem

$$\begin{aligned} 0 &= -y + r^2 + \mathcal{R}_r(r, \theta, y, 0, 0), \\ \dot{\theta} &= \sigma, \\ \dot{y} &= -1 + \mathcal{R}_y(r, \theta, y, 0, 0). \end{aligned} \tag{16}$$

In this case there is no slow variable, and therefore no parameter in system (16). This is natural because in case (C2), system (11) only has two (as opposed to three) time-scales.

The reduced problem in case (C3)

In this case we rewrite system (11) on the slow time-scale $\tau_{\varepsilon_2} = \varepsilon_2 t$, thereby obtaining system (15). Since $\varepsilon_1/\varepsilon_2 \ll 1$, taking the double singular limit $(\varepsilon_1, \varepsilon_2) \rightarrow (0, 0)$ leads to the reduced problem

$$\begin{aligned} 0 &= -y + r^2 + \mathcal{R}_r(r, \theta, y, 0, 0), \\ \dot{\theta} &= 0, \\ \dot{y} &= -1 + \mathcal{R}_y(r, \theta, y, 0, 0). \end{aligned} \tag{17}$$

This time, the angular variable θ is the slow variable to be considered as a parameter in system (16). Thus singular orbits obtained as concatenations of layer and reduced orbit segments are contained within constant θ planes. As a result, the reduced problem (16) is in 1-1 correspondence with the reduced problem associated with the normal form of the regular fold point in [37]. This case is sketched in Figure 2.

For $0 < \varepsilon_1, \varepsilon_2 \ll 1$, Fenichel-Tikhonov theory implies that compact submanifolds of the normally hyperbolic critical manifolds S_0^a and S_0^r persist as $\mathcal{O}(l(\varepsilon_1, \varepsilon_2))$ -close locally invariant *slow manifolds* $S_{l(\varepsilon_1, \varepsilon_2)}^a$ and $S_{l(\varepsilon_1, \varepsilon_2)}^r$ respectively [16, 26, 40, 57, 58], where we write $l(\varepsilon_1, \varepsilon_2) := \max\{\varepsilon_1, \varepsilon_2\}$ in order to keep the discussion general, i.e. so that we need not distinguish between cases (C1), (C2) and (C3). Our goal is to describe the extension of the attracting slow manifold $S_{l(\varepsilon_1, \varepsilon_2)}^a$ through a neighbourhood of the non-hyperbolic cycle S_0^c corresponding to the regular folded cycle in system (11).

Remark 2.4. In [9], the authors extend GSPT for a class of multiple time-scale systems with $n \geq 3$ time-scales which feature ‘nested critical manifolds’. A requirement for the application of this theory to system (7) is that the reduced problem on S_0 has a one-dimensional critical manifold. This condition is not satisfied in any case (C1), (C2) or (C3) because none of the reduced problems (14), (16) and (17) have equilibria in the neighbourhood of interest (i.e. close to $r = y = 0$).

3 Main Results

We now state and describe our main results. In order to distinguish the different cases (C1), (C2) and (C3), we scale ε_1 and ε_2 by a single small parameter $\varepsilon \ll 1$. Main results are stated and proved for the simplified normal form (11) with $\varepsilon_1 = \varepsilon^\alpha$ and $\varepsilon_2 = \varepsilon^3$, i.e. for the system

$$\begin{aligned} r' &= r^2 - y + \tilde{\mathcal{R}}_r(r, \theta, y, \varepsilon), \\ \theta' &= \varepsilon^\alpha, \\ y' &= \varepsilon^3(-1 + \tilde{\mathcal{R}}_y(r, \theta, y, \varepsilon)), \end{aligned} \tag{18}$$

where $\tilde{\mathcal{R}}_r(r, \theta, y, \varepsilon) = \mathcal{O}(r^3, y^2, ry, \varepsilon^3)$ and $\tilde{\mathcal{R}}_y(r, \theta, y, \varepsilon) = \mathcal{O}(r, y, \varepsilon^3)$. The different cases (C1), (C2) and (C3) are obtained for different values of the scaling parameter $\alpha \in \mathbb{R}_{\geq 1}$ as follows:

- Case (C1)*: $\alpha = 1$;
- Case (C1): $\alpha \in (1, 3)$;
- Case (C2): $\alpha = 3$;
- Case (C3): $\alpha > 3$.

Note that we have introduced an additional case (C1)*. This case is dynamically distinct from the others, but it is not distinguished in Section 2 because the geometry and dynamics in the double singular limit are the same as for case (C1).

Remark 3.1. The choice to write ε^3 instead of ε in the equation for y is made a-posteriori in order to avoid fractional exponents in the proofs. Comparisons with known results for the stationary regular fold point in [37] are possible via the simple relation $\varepsilon_{\text{KS}} = \varepsilon^3$, where we denote by ε_{KS} the small parameter in [37]. Similar observations motivated the use of a cubic exponent for the small parameter in other works involving folded singularities, e.g. in [48, 49].

Our aim is to describe the forward evolution of initial conditions in an annular entry section

$$\Delta^{\text{in}} := \left\{ (r, \theta, R^2) : \left| -1 + \frac{r}{R} \right| \leq \beta, \theta \in \mathbb{R}/\mathbb{Z} \right\}, \quad (19)$$

where R and β are small positive constants. We track solutions of system (18) up to their intersection with the cylindrical exit section

$$\Delta^{\text{out}} := \{ (R, \theta, y) : \theta \in \mathbb{R}/\mathbb{Z}, y \in [-y_0, y_0] \}, \quad (20)$$

for a small positive constant $y_0 > 0$. The critical manifold S_0 , the Fenichel slow manifolds and the entry/exit sections are visualized in the (r, y) -plane in Figure 3 and in the three-dimensional space in Figure 4.

We now state the main result, which characterises the dynamics of the map $\pi : \Delta^{\text{in}} \rightarrow \Delta^{\text{out}}$ induced by the flow of system (18) in cases (C1)*, (C1), (C2) and (C3).

Theorem 3.2. *Consider system (18) with $\alpha \geq 1$. There exists an $\varepsilon_0 > 0$ such that for all $\varepsilon \in (0, \varepsilon_0]$, the map $\pi : \Delta^{\text{in}} \rightarrow \Delta^{\text{out}}$ is at least C^1 -smooth with the following properties:*

(a) (Asymptotics). $\pi : (r, \theta, R^2) \mapsto (R, h_\theta(r, \theta, \varepsilon), h_y(r, \theta, \varepsilon))$, where

$$\begin{aligned} h_\theta(r, \theta, \varepsilon) &= \theta + (R^2 \varepsilon^{\alpha-3} + \Omega_0 \varepsilon^{\alpha-1}) (1 + \mathcal{O}(R)) + \mathcal{O}(\varepsilon^\alpha \ln \varepsilon) \pmod{1}, \\ h_y(r, \theta, \varepsilon) &= -\Omega_0 \varepsilon^2 + \mathcal{O}(\varepsilon^3 \ln \varepsilon), \end{aligned}$$

as $\varepsilon \rightarrow 0$. Here $\mathcal{O}(R)$ denotes a correction with $|\mathcal{O}(R)| \leq CR$ for a constant $C > 0$, and the constant $\Omega_0 > 0$ is the smallest positive zero of $J_{-1/3}(2z^{3/2}/3) + J_{1/3}(2z^{3/2}/3)$ where $J_{\pm 1/3}$ are Bessel functions of the first kind. In particular,

$$\pi(S_\varepsilon^{\text{a}} \cap \Delta^{\text{in}}) = \{ (R, \theta, -\Omega_0 \varepsilon^2 + \mathcal{O}(\varepsilon^3 \ln \varepsilon)) : \theta \in \mathbb{R}/\mathbb{Z} \}.$$

(b) (Strong contraction). *The y -component of $\pi(r, \theta, R^2)$ is a strong contraction with respect to r . More precisely,*

$$\frac{\partial h_y}{\partial r}(r, \theta, \varepsilon) = \mathcal{O}\left(e^{-\kappa/\varepsilon^3}\right)$$

for a constant $\kappa \in (0, 4R^2/3)$ as $\varepsilon \rightarrow 0$.

Theorem 3.2 characterises the asymptotic behaviour of solutions and the extension of the attracting Fenichel slow manifold S_ε^{a} through a neighbourhood of the regular folded cycle in the normal form (18). The geometry and dynamics for all four cases (C1)*, (C1), (C2) and (C3) are sketched in Figures 5, 6, 7 and 8 respectively. The proof is based on the blow-up method, and deferred to Section 4.

The asymptotics in Assertion (a) hold for all $\alpha \geq 1$, i.e. in all cases (C1)*, (C1), (C2) and (C3). The asymptotics for the parameter drift in y are the same as for the stationary regular fold point, at least up to $\mathcal{O}(\varepsilon^3 \ln \varepsilon)$, since

$$h_y(r, \theta, \varepsilon) = h_y\left(r, \theta, \varepsilon_{\text{KS}}^{1/3}\right) = -\Omega_0 \varepsilon_{\text{KS}}^{2/3} + \mathcal{O}(\varepsilon_{\text{KS}} \ln \varepsilon_{\text{KS}})$$

agrees with the asymptotic estimates in [37, 46] (recall from Remark 3.1 that $\varepsilon_{\text{KS}} = \varepsilon^3$, where ε_{KS} denotes the small parameter in [37]). Similarly, the strong contraction property described in Assertion (b) does not depend on α . This explains the similarity between the dynamics observed in the (r, y) -plane and the dynamics near a stationary regular fold point; c.f. Figure 3 and [37, Fig. 2.1]. The dynamics in different cases, i.e. for differing values of α , are primarily distinguished via the angular dynamics and in particular, the number of complete rotations about the y -axis during the transition from Δ^{in} to Δ^{out} . Since $\theta \in \mathbb{R}/\mathbb{Z}$, a solution with initial condition $(r, \theta, R) \in \Delta^{\text{in}}$ undergoes a total of

$$N_{\text{rot}}(\varepsilon, \alpha) = \lfloor R^2 (\varepsilon^{\alpha-3} + \Omega_0 \varepsilon^{\alpha-1}) (1 + \mathcal{O}(R)) + \mathcal{O}(\varepsilon^\alpha \ln \varepsilon) \rfloor$$

rotations about the y -axis. This yields the following in cases (C1)*, (C1), (C2) and (C3):

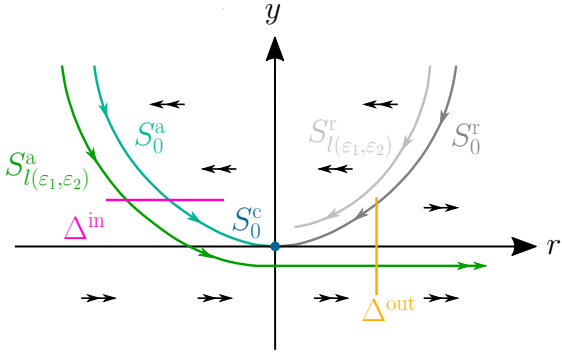


Figure 3: Projected geometry and dynamics in the (r, y) -plane, as described by Theorem 3.2. The critical manifold and its submanifolds are shown in colours consistent with earlier figures. The entry, exit sections Δ^{in} , Δ^{out} (magenta, orange) and the (extended) Fenichel slow manifolds $S_{l(\epsilon_1, \epsilon_2)}^a$, $S_{l(\epsilon_1, \epsilon_2)}^r$ are also shown, in green and light shaded grey respectively. Since the asymptotics in the y -component described in Assertion (a) and the strong contractivity described in Assertion (b) agree with corresponding results for the stationary regular fold point, the dynamics in the (r, y) -plane agrees qualitatively with [37, Fig. 2.1].

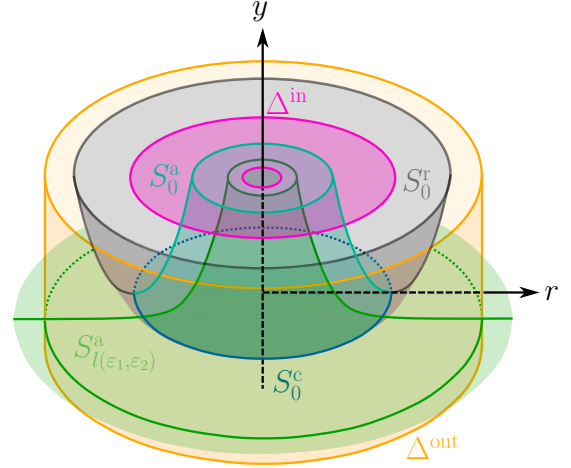


Figure 4: The extension of the attracting slow manifold $S_{l(\epsilon_1, \epsilon_2)}^a$ (again in shaded green) as described by Theorem 3.2, in the full (r, θ, y) -space. The entry, exit sections Δ^{in} , Δ^{out} as well as the critical manifold and its submanifolds are also shown, with the same colouring as in Figure 3. The intersection $\pi(S_{l(\epsilon_1, \epsilon_2)}^a) \cap \Delta^{\text{in}} \subset \Delta^{\text{out}}$ is topologically equivalent to a circle (shown in dark green), and $O(\epsilon^2)$ -close to the plane $\{y = 0\}$ in the Hausdorff distance. The specific behaviour of solutions, which depends on α , is not shown (see however Figures 5, 6, 7 and 8 below).

(C1)* $N_{\text{rot}}(\epsilon, 1) = \lfloor R^2(\epsilon^{\alpha-3} + \Omega_0 \epsilon^{\alpha-1})(1 + \mathcal{O}(R)) \rfloor = \lfloor \mathcal{O}(\epsilon^{-2}) \rfloor$, see Figure 5.

(C1) $N_{\text{rot}}(\epsilon, \alpha) = \lfloor R^2(\epsilon^{\alpha-3} + \Omega_0 \epsilon^{\alpha-1})(1 + \mathcal{O}(R)) \rfloor = \lfloor \mathcal{O}(\epsilon^{\alpha-3}) \rfloor$, where $\alpha - 3 \in (-2, 0)$. See Figure 6.

(C2) $N_{\text{rot}}(\epsilon, 3) = \lfloor R^2(1 + \mathcal{O}(R)) + \mathcal{O}(\epsilon^3 \ln \epsilon) \rfloor$, see Figure 7.

(C3) $N_{\text{rot}}(\epsilon, \alpha) = 0$, see Figure 8.

Each case is clearly distinguished within the blow-up analysis in Section 4, where it is shown that the $\mathcal{O}(\epsilon^{\alpha-3})$, $\mathcal{O}(\epsilon^{\alpha-1})$ and $\mathcal{O}(\epsilon^\alpha \ln \epsilon)$ terms correspond to the rotation undergone by solutions during their approach to an ϵ -dependent neighbourhood of S_0^c , their passage through this neighbourhood, and their departure from it respectively. Full rotations about the y -axis may or may not be observed during the approach and passage through this neighbourhood, depending on the case (C1)*, (C1), (C2) or (C3).

4 Proof of Theorem 3.2

Our aim is to investigate the three time-scale system (18) using the blow-up method developed for fast-slow systems in [14, 37, 38, 39]; we refer again to [24] for a recent survey. Many aspects of the proof rely in particular on arguments used in the blow-up analysis of the (stationary) regular fold point in [37]. We adopt the (now well established) notational conventions introduced in [37, 38, 39].

The blow-up transformation is defined in Section 4.1, as are the three local coordinate charts that we use for calculations. The geometry and dynamics in all three coordinate charts are considered in turn in Sections 4.2, 4.3 and 4.4. Theorem 3.2 is proved in Section 4.5 using the information obtained in local coordinate charts.

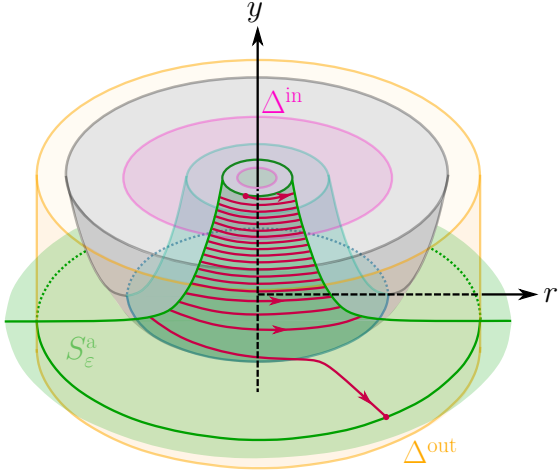


Figure 5: Case (C1)*. Sketch of the flow of system (18) for $\alpha = 1$. The solution sketched in red makes $N_{\text{rot}}(\varepsilon, 1) = \lfloor \mathcal{O}(\varepsilon^{-2}) \rfloor$ rotations about the y -axis before leaving the neighbourhood close to $S_\varepsilon^a \cap \Delta^{\text{out}}$ at an angle approximated by the expression for $h_\theta(r, \theta, \varepsilon)$ in Theorem 3.2 Assertion (a).

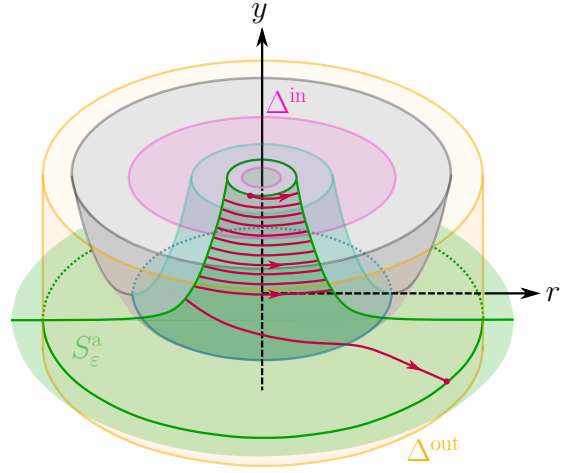


Figure 6: Case (C1). Sketch of the flow of system (18) for $1 < \alpha < 3$. The solution sketched in red makes $N_{\text{rot}}(\varepsilon, \alpha) = \lfloor \mathcal{O}(\varepsilon^{\alpha-3}) \rfloor$ rotations about the y -axis before leaving the neighbourhood close to $S_\varepsilon^a \cap \Delta^{\text{out}}$ at an angle approximated by the expression for $h_\theta(r, \theta, \varepsilon)$ in Theorem 3.2 Assertion (a).

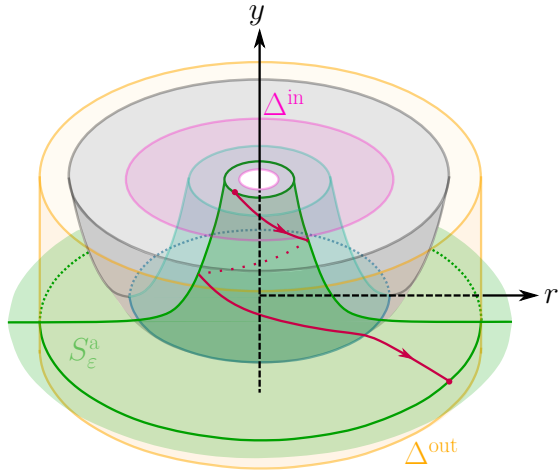


Figure 7: Case (C2). Sketch of the flow of system (18) for $\alpha = 3$. The solution sketched in red makes $N_{\text{rot}}(\varepsilon, \alpha) = \lfloor R^2(1 + \mathcal{O}(R)) + \mathcal{O}(\varepsilon^3 \ln \varepsilon) \rfloor$ rotations about the y -axis before leaving the neighbourhood close to $S_\varepsilon^a \cap \Delta^{\text{out}}$ at an angle approximated by the expression for $h_\theta(r, \theta, \varepsilon)$ in Theorem 3.2 Assertion (a).

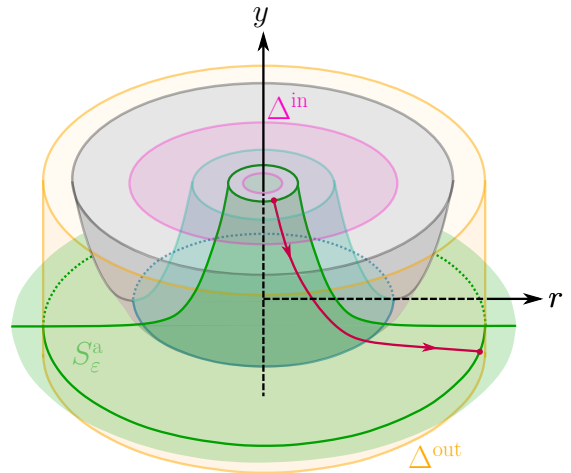


Figure 8: Case (C3). Sketch of the flow of system (18) for $\alpha > 3$. The solution sketched in red makes $N_{\text{rot}}(\varepsilon, \alpha) = 0$ rotations about the y -axis before leaving the neighbourhood close to $S_\varepsilon^a \cap \Delta^{\text{out}}$ at an angle approximated by the expression for $h_\theta(r, \theta, \varepsilon)$ in Theorem 3.2 Assertion (a).

4.1 Blow-up and local coordinate charts

As is standard in blow-up approaches, we consider the extended system obtained from (18) after appending the trivial equation $\varepsilon' = 0$, i.e.

$$\begin{aligned} r' &= -y + r^2 + \widetilde{\mathcal{R}}_r(r, \theta, y, \varepsilon), \\ \theta' &= \varepsilon^\alpha, \\ y' &= \varepsilon^3(-1 + \widetilde{\mathcal{R}}_y(r, \theta, y, \varepsilon)), \\ \varepsilon' &= 0, \end{aligned} \tag{21}$$

where $\widetilde{\mathcal{R}}_r(r, \theta, y, \varepsilon) = \mathcal{O}(r^3, y^2, ry, \varepsilon^3)$ and $\widetilde{\mathcal{R}}_y(r, \theta, y, \varepsilon) = \mathcal{O}(r, y, \varepsilon^3)$.

In order to describe the map $\pi : \Delta^{\text{in}} \rightarrow \Delta^{\text{out}}$, we introduce extended entry and exit sections

$$\Delta_\varepsilon^{\text{in}} := \left\{ (r, \theta, R^2, \varepsilon) : \left| -1 + \frac{r}{R} \right| \leq \beta, \theta \in \mathbb{R}/\mathbb{Z}, \varepsilon \in [0, \varepsilon_0] \right\}, \tag{22}$$

and

$$\Delta_\varepsilon^{\text{out}} := \{ (R, \theta, y, \varepsilon) : \theta \in \mathbb{R}/\mathbb{Z}, y \in [-y_0, y_0], \varepsilon \in [0, \varepsilon_0] \}, \tag{23}$$

respectively. The entry, exit sections Δ^{in} , Δ^{out} defined in Section 3 (recall equations (19) and (20)) can be viewed as constant ε sections of $\Delta_\varepsilon^{\text{in}}$, $\Delta_\varepsilon^{\text{out}}$ respectively. Based on this simple relationship, we study the map $\pi : \Delta^{\text{in}} \rightarrow \Delta^{\text{out}}$ described in Theorem 3.2 via the extended map $\pi_\varepsilon : \Delta_\varepsilon^{\text{in}} \rightarrow \Delta_\varepsilon^{\text{out}}$ induced by the flow of initial conditions in $\Delta_\varepsilon^{\text{in}}$ up to $\Delta_\varepsilon^{\text{out}}$ under system (21).

We now define the relevant blow-up transformation. Let $I = [0, P]$ for a fixed $P \in (0, \bar{v})$, let

$$B_0 := S^2 \times \mathbb{R}/\mathbb{Z} \times [0, P],$$

and define the (weighted) blow-up transformation via

$$\varphi : B_0 \rightarrow \mathbb{R}_{\geq -\bar{v}} \times \mathbb{R}/\mathbb{Z} \times \mathbb{R} \times \mathbb{R}_{\geq 0}, \quad (\bar{r}, \bar{y}, \bar{\varepsilon}, \theta, \rho) \mapsto (r, \theta, y, \varepsilon) = (\rho \bar{r}, \theta, \rho^2 \bar{y}, \rho \bar{\varepsilon}), \tag{24}$$

where $(\bar{r}, \bar{y}, \bar{\varepsilon}) \in S^2$. The blow-up map φ is a diffeomorphism for $\rho \in (0, P]$, but not for $\rho = 0$. In particular, the preimage of the non-hyperbolic cycle S_0^* under φ is a ‘torus of spheres’ $S^2 \times \mathbb{R}/\mathbb{Z} \times \{0\} \cong S^2 \times S^1$.

For calculational purposes, we introduce local coordinate charts in order to describe the dynamics on

$$B_{\bar{y}}^+ := B_0 \cap \{\bar{y} > 0\}, \quad B_{\bar{\varepsilon}}^+ := B_0 \cap \{\bar{\varepsilon} > 0\}, \quad B_{\bar{r}}^+ := B_0 \cap \{\bar{r} > 0\}.$$

Following [37], we introduce affine projective coordinates via

$$\begin{aligned} K_1 : B_{\bar{y}}^+ &\rightarrow \mathbb{R} \times \mathbb{R}/\mathbb{Z} \times \mathbb{R} \times \mathbb{R}, & (\bar{r}, \bar{y}, \bar{\varepsilon}, \rho, \theta) &\mapsto (r_1, \theta_1, \rho_1, \varepsilon_1) = (\bar{r} \bar{y}^{-\frac{1}{2}}, \theta, \rho \bar{y}^{\frac{1}{2}}, \bar{\varepsilon} \bar{y}^{-\frac{1}{2}}), \\ K_2 : B_{\bar{\varepsilon}}^+ &\rightarrow \mathbb{R} \times \mathbb{R}/\mathbb{Z} \times \mathbb{R} \times \mathbb{R}, & (\bar{r}, \bar{y}, \bar{\varepsilon}, \rho, \theta) &\mapsto (r_2, \theta_2, y_2, \rho_2) = (\bar{r} \bar{\varepsilon}^{-1}, \theta, \bar{y} \bar{\varepsilon}^{-2}, \rho \bar{\varepsilon}), \\ K_3 : B_{\bar{r}}^+ &\rightarrow \mathbb{R} \times \mathbb{R}/\mathbb{Z} \times \mathbb{R} \times \mathbb{R}, & (\bar{r}, \bar{y}, \bar{\varepsilon}, \rho, \theta) &\mapsto (\rho_3, \theta_3, y_3, \varepsilon_3) = (\rho \bar{r}, \theta, \bar{y} \bar{r}^{-2}, \bar{\varepsilon} \bar{r}^{-1}). \end{aligned}$$

Here we permit a small abuse of notation by introducing a new variable ε_1 , which should not be confused with the small parameter with the same notation in Sections 1-2. This leads to the following coordinates:

$$\begin{aligned} K_1 : (r, \theta, y, \varepsilon) &= (\rho_1 r_1, \theta_1, \rho_1^2 \varepsilon_1), \\ K_2 : (r, \theta, y, \varepsilon) &= (\rho_2 r_2, \theta_2, \rho_2^2 y_2, \rho_2), \\ K_3 : (r, \theta, y, \varepsilon) &= (\rho_3, \theta_3, \rho_3^2 y_3, \rho_3 \varepsilon_3). \end{aligned} \tag{25}$$

In the analysis, it will be necessary to change coordinates between different charts. The following lemma provides the relevant change of coordinates formulae.

Lemma 4.1. *The change of coordinate maps κ_{ij} from K_i to K_j are diffeomorphisms given by*

$$\begin{aligned} \kappa_{12} : & \quad r_2 = r_1 \varepsilon_1^{-1}, & \theta_2 &= \theta_1, & y_2 &= \varepsilon_1^{-2}, & \rho_2 &= \rho_1 \varepsilon_1, & \text{for } \varepsilon_1 > 0, \\ \kappa_{12}^{-1} : & \quad r_1 = r_2 y_2^{-\frac{1}{2}}, & \theta_1 &= \theta_2, & \rho_1 &= \rho_2 y_2^{\frac{1}{2}}, & \varepsilon_1 &= y_2^{-\frac{1}{2}}, & \text{for } y_2 > 0, \\ \kappa_{23} : & \quad \rho_3 = \rho_2 r_2, & \theta_3 &= \theta_2, & y_3 &= y_2 r_2^{-2}, & \varepsilon_3 &= r_2^{-1}, & \text{for } r_2 > 0, \\ \kappa_{23}^{-1} : & \quad r_2 = \varepsilon_3^{-1}, & \theta_2 &= \theta_3, & y_2 &= y_3 \varepsilon_3^{-2}, & \rho_2 &= \rho_3 \varepsilon_3, & \text{for } \varepsilon_3 > 0. \end{aligned} \tag{26}$$

Proof. This follows from the local coordinate expressions in (25). \square

Remark 4.2. The angular variable θ is non-local and unaffected by the blow-up transformation (24). It follows that φ can be defined more succinctly in terms of its action on the remaining variables, i.e. via the map

$$S^2 \times [0, P] \rightarrow \mathbb{R}_{\geq -\bar{v}} \times \mathbb{R} \times \mathbb{R}_{\geq 0}, \quad (\bar{r}, \bar{y}, \bar{\varepsilon}, \rho) \mapsto (r, y, \varepsilon) = (\rho\bar{r}, \rho^2\bar{y}, \rho\bar{\varepsilon}),$$

which is precisely the blow-up map used to study the regular fold point in [37] (recall that $\varepsilon_{\text{KS}} = \varepsilon^3$ by the discussion following the statement of Theorem 3.2).

Remark 4.3. By construction, the blown-up vector field induced by the pushforward of the vector field induced by system (21) under φ is invariant in the hyperplanes $\{\rho = 0\}$ and $\{\bar{\varepsilon} = 0\}$. The former corresponds to blown-up preimage of the non-hyperbolic cycle S_0^c , i.e. the torus of spheres $S^2 \times S^1$. The latter contains the blown-up preimage of the critical manifold S_0 . Since $\bar{r}^2 + \bar{y}^2 = 1$ in $\{\bar{\varepsilon} = 0\}$, the preimage of φ in $\{\bar{\varepsilon} = 0\}$ is $S^1 \times \mathbb{R}/\mathbb{Z} \times \mathbb{R}_{\geq 0} \cong S^1 \times S^1 \times \mathbb{R}_{\geq 0}$. Thus, the part of the blown-up singular cycle S_0^c within $\{\bar{\varepsilon} = 0\}$ is a torus.

Remark 4.4. Since $\varepsilon = \text{const.}$ in system (21) we have constants of the motion defined by $\varepsilon = \rho_1\varepsilon_1$, $\varepsilon = \rho_2$, $\varepsilon = \rho_3\varepsilon_3$ in charts K_1 , K_2 , K_3 respectively.

Remark 4.5. The blow-up transformation (24) can also be used to study the dynamics of the full normal form in Proposition 2.1 with $(\varepsilon_1, \varepsilon_2) = (\varepsilon^\alpha, \varepsilon^3)$, for all $\alpha \geq 1$. Assumption 3 is expected to be the most restrictive in the case (C1)* with $\alpha = 1$, since extra terms $\varepsilon_1 a(\theta, \varepsilon_1)r$ and $\varepsilon_1 c(\theta, \varepsilon_1)$ in system (7) influence the dynamics after desingularization on the blow-up surface $S^2 \times S^1$. For all other cases with $\alpha > 1$, these additional terms are pushed to higher orders, i.e. they vanish for $\rho = 0$. Thus one expects the dynamics to be similar to those of the simplified normal form (11) in cases (C1), (C2) and (C3). A rigorous treatment of the full normal form and a corresponding proof of these claims is left for future work.

We turn now to the dynamics in charts K_i , $i = 1, 2, 3$.

4.2 Dynamics in the entry chart K_1

In chart K_1 we analyse solutions which track the blown-up preimage of the attracting Fenichel slow manifold S_ε^a as they enter a neighbourhood of the non-hyperbolic circle S_0^c .

Lemma 4.6. Following the positive transformation of time $\rho_1 dt = dt_1$, the desingularized equations in chart K_1 are given by

$$\begin{aligned} r_1' &= r_1^2 - 1 + \frac{1}{2}\varepsilon_1^3 r_1 + \mathcal{O}(\rho_1), \\ \theta_1' &= \rho_1^{\alpha-1} \varepsilon_1^\alpha, \\ \rho_1' &= \frac{1}{2}\rho_1 \varepsilon_1^3 (-1 + \mathcal{O}(\rho_1)), \\ \varepsilon_1' &= \frac{1}{2}\varepsilon_1^4 (1 + \mathcal{O}(\rho_1)), \end{aligned} \tag{27}$$

where by a slight abuse of notation we now write $(\cdot)' = d/dt_1$.

Proof. This follows after direct differentiation of the local coordinate expressions in (25) and subsequent application of the desingularization $\rho_1 dt = dt_1$. \square

The analysis in chart K_1 is restricted to the set

$$\mathcal{D}_1 := \{(r_1, \theta_1, \rho_1, \varepsilon_1) \in \mathbb{R} \times \mathbb{R}/\mathbb{Z} \times \mathbb{R} \times \mathbb{R} : 0 \leq \rho_1 \leq R, 0 \leq \varepsilon_1 \leq E\},$$

where R is the constant which defines the entry set Δ^{in} in (19) and $E = \varepsilon_0/R > 0$ due to the relationship $\varepsilon = \rho_1\varepsilon_1$ (recall Remark 4.4). The set \mathcal{D}_1 is sketched with other geometric and dynamical objects in chart K_1 in Figure 9.

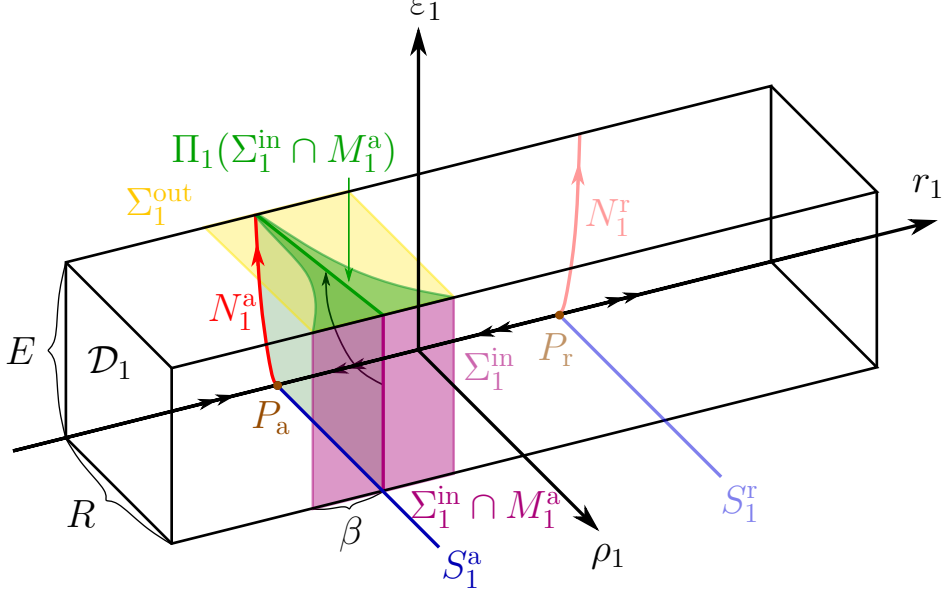


Figure 9: Geometry and dynamics within \mathcal{D}_1 , shown in $(r_1, \rho_1, \varepsilon_1)$ -space. Projections of the two-dimensional attracting and repelling critical manifolds $S_1^a, S_1^r \subset \{\varepsilon_1 = 0\}$ (shown in blue and shaded blue) extend up to their intersection with the blow-up surface at $P_a, P_r \subset \{\rho_1 = \varepsilon_1 = 0\}$ respectively. Projections of the two-dimensional center manifolds $N_1^a, N_1^r \subset \{\rho_1 = 0\}$ emanating from P_a, P_r , as described in Lemma 4.7, are shown in red and shaded red. Entry and exit sections Σ_1^{in} and Σ_1^{out} are shown in shaded magenta and yellow respectively. The projected three-dimensional center manifold M_1^a and its image under Π_1 is described by Proposition 4.11. This is shown along with the image $\Pi_1(\Sigma_1^{\text{in}}) \subset \Sigma_1^{\text{out}}$ in green.

System (27) is well-defined within $\{\rho_1 = 0\}$ (recall that $\alpha \geq 1$), which corresponds to the part of the blow-up surface in K_1 . The subspace $\{\varepsilon_1 = 0\}$ is also invariant, and contains two two-dimensional critical manifolds

$$S_1^a := \{(r_1, \theta_1, \rho_1, \varepsilon) \in \mathcal{D}_1 : r_1 = -1 + \mathcal{O}(\rho_1)\}, \quad S_1^r := \{(r_1, \theta_1, \rho_1, \varepsilon) \in \mathcal{D}_1 : r_1 = 1 + \mathcal{O}(\rho_1)\}, \quad (28)$$

which correspond to the blown-up preimages of the critical manifolds S_0^a and S_0^r in chart K_1 respectively. Both S_1^a and S_1^r are topologically equivalent to cylindrical segments, and they are normally hyperbolic and attracting resp. repelling up to and including the circular sets

$$P_a := \{(-1, \theta_1, 0, 0) : \theta_1 \in \mathbb{R}/\mathbb{Z}\}, \quad P_r := \{(1, \theta_1, 0, 0) : \theta_1 \in \mathbb{R}/\mathbb{Z}\},$$

which intersect with the blow-up surface; see Figures 9 and 10. The linearisation of system (27) along P_a is

$$J(P_a) = \begin{pmatrix} -2 & 0 & 0 & 0 \\ 0 & 0 & 0 & 0^{\alpha-1} \\ 0 & 0 & 0 & 0 \\ 0 & 0 & 0 & 0 \end{pmatrix}. \quad (29)$$

Note that $0^{\alpha-1} = 0$ for all $\alpha > 1$, but $0^{\alpha-1} = 1$ if $\alpha = 1$. In both cases, the set P_a is partially hyperbolic with a single non-trivial eigenvalue -2 and corresponding eigenvector $(1, 0, 0, 0)$. The remaining three eigenvalues along P_a are identically zero, with eigenvectors $(0, 1, 0, 0)$, $(0, 0, 1, 0)$ and $(0, 0, 0, 1)$ (the latter is a generalized eigenvector if $\alpha = 1$). Thus in the blown-up space (i.e. for system (27)), we have regained partial hyperbolicity. This allows us to extend the attracting center manifold with base along S_1^a up onto the blow-up surface using center manifold theory.

Lemma 4.7. *Consider system (27) on \mathcal{D}_1 with $E, R > 0$ sufficiently small. There exists a three-dimensional center-stable manifold M_1^a such that*

$$M_1^a|_{\varepsilon_1=0} = S_1^a, \quad M_1^a|_{\rho_1=0} = N_1^a,$$

where $S_1^a \subset \{\varepsilon_1 = 0\}$ is the two-dimensional attracting critical manifold in (28) and $N_1^a \subset \{\rho_1 = 0\}$ is a unique two-dimensional center-stable manifold for the restricted system (27)| $_{\rho_1=0}$ emanating from P_a . The manifold M_1^a is given locally as a smooth graph $r_1 = h_{r_1}(\theta_1, \rho_1, \varepsilon_1)$, where

$$h_{r_1}(\theta_1, \rho_1, \varepsilon_1) = -1 - \frac{1}{4}\varepsilon_1^3 + \mathcal{O}(\rho_1, \varepsilon_1^6). \quad (30)$$

There exists a constant $c \in (-2, 0)$ such that initial conditions in Σ_1^{in} are attracted to M_1^a along one-dimensional stable fibers faster than e^{-ct_1} .

Proof. The existence of a three-dimensional center manifold M_1^a follows from the linearisation (29) and center manifold theory [43]. The fact that M_1^a contains two-dimensional manifolds N_1^a and S_1^a with the properties described follows after direct restriction to the invariant hyperplanes $\{\rho_1 = 0\}$ and $\{\varepsilon_1 = 0\}$ respectively.

The graph representation in (30) is obtained using the standard approach based on formal matching. More precisely, we substitute a power series ansatz of the form

$$r_1 = h_{r_1}(\theta_1, \rho_1, \varepsilon_1) = \sum_{n=0}^{\infty} a_n(\theta_1)\varepsilon_1^n + \mathcal{O}(\rho_1)$$

into the equation for r_1 in system (27) and determine the coefficients $a_n(\theta_1)$ by comparing

$$\begin{aligned} r_1' &= \sum_{n=0}^{\infty} \left(\frac{da_n(\theta_1)}{d\theta_1} \theta_1' \varepsilon_1^n + a_{n+1}(\theta_1)(n+1)\varepsilon_1^n \varepsilon_1' \right) + \mathcal{O}(\rho_1) \\ &= \frac{1}{2} \sum_{n=0}^{\infty} \left(\frac{da_n(\theta_1)}{d\theta_1} \rho_1^{\alpha-1} \varepsilon_1^{n+\alpha} + a_{n+1}(\theta_1)(n+1)\varepsilon_1^{n+4} \right) + \mathcal{O}(\rho_1), \end{aligned}$$

with

$$\begin{aligned} r_1' &= \left(\sum_{n=0}^{\infty} a_n(\theta_1)\varepsilon_1^n \right)^2 - 1 + \frac{1}{2}\varepsilon_1^3 \sum_{n=0}^{\infty} a_n(\theta_1)\varepsilon_1^n + \mathcal{O}(\rho_1) \\ &= \sum_{n=0}^{\infty} \left(\sum_{k=0}^n a_k(\theta_1)a_{n-k}(\theta_1) \right) \varepsilon_1^n - 1 + \frac{1}{2} \sum_{n=0}^{\infty} a_n(\theta_1)\varepsilon_1^{n+3} + \mathcal{O}(\rho_1). \end{aligned}$$

The details are omitted for brevity.

The strong contraction along stable fibers at a rate greater than e^{-ct_1} for some $c \in (0, 2)$ follows from Fenichel theory [16, Theorem 9.1] and the fact that the stable leading eigenvalue is $\lambda = -2$, recall (29). \square

The two-dimensional center manifold N_1^a is sketched within $\{\rho_1 = 0\}$ in Figure 11.

Remark 4.8. *Similar to Lemma 4.7, there exists a three-dimensional center-unstable manifold M_1^r at P_r that contains the repelling critical manifold $S_1^r \subset \{\varepsilon_1 = 0\}$ and a repelling center manifold $N_1^r \subset \{\rho_1 = 0\}$. These objects are shown in Figures 10 and 11. In \mathcal{D}_1 , the manifold M_1^r is given as a smooth graph $r_1 = \tilde{h}_{r_1}(\theta_1, \rho_1, \varepsilon_1)$, where*

$$\tilde{h}_{r_1}(\theta_1, \rho_1, \varepsilon_1) = 1 - \frac{1}{4}\varepsilon_1^3 + \mathcal{O}(\varepsilon_1^6, \rho_1).$$

In contrast to N_1^a , the manifold N_1^r is not unique. We omit the explicit treatment of the dynamics near M_1^r since it is not relevant to the proof of Theorem 3.2.

Lemma 4.7 can be used to describe the r_1 -component of the map $\Pi_1 : \Sigma_1^{\text{in}} \rightarrow \Sigma_1^{\text{out}}$ induced by the flow of initial conditions in

$$\Sigma_1^{\text{in}} := \{(r_1, \theta_1, R, \varepsilon_1) \in \mathcal{D}_1 : |r_1 + 1| \leq \beta\},$$

i.e. the representation of the entry section Δ_e^{in} defined in (22) in K_1 coordinates, up to the exit section

$$\Sigma_1^{\text{out}} := \{(r_1, \theta_1, \rho_1, E) \in \mathcal{D}_1 : |r_1 + 1| \leq \beta\}.$$

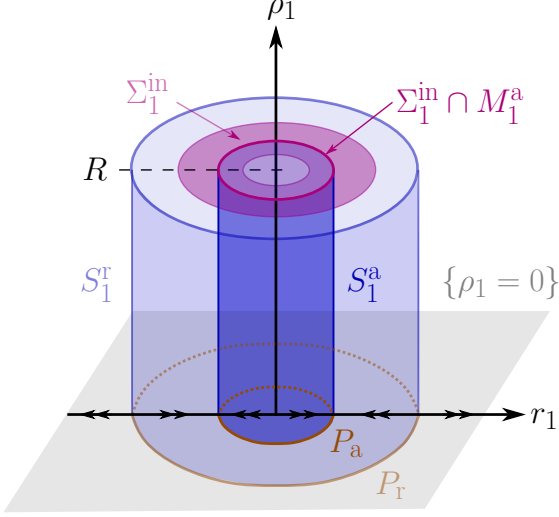


Figure 10: Geometry and dynamics within the invariant hyperplane $\{\varepsilon_1 = 0\}$, projected into (r_1, θ_1, ρ_1) -space; c.f. Figure 9.

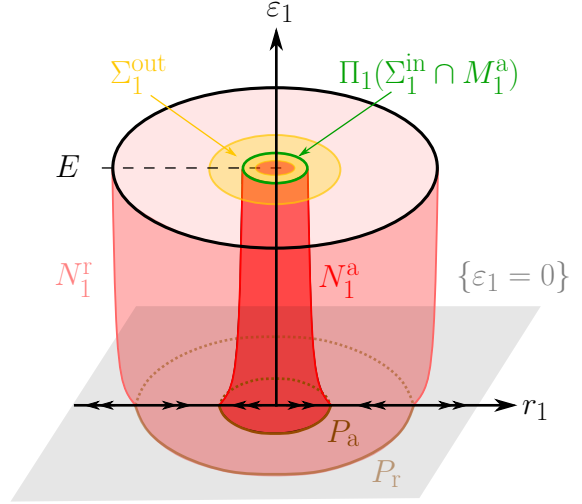


Figure 11: Geometry and dynamics within the invariant hyperplane $\{\rho_1 = 0\}$, projected into $(r_1, \theta_1, \varepsilon_1)$ -space; c.f. Figures 9 and 10.

The remaining θ_1 , ρ_1 and ε_1 components of the map Π_1 can be calculated directly using explicit solution formulae and the transition time taken for solutions with initial conditions in Σ_1^{in} to reach Σ_1^{out} . These expressions are provided by the following result (c.f. [37, Lemma 2.7]).

Lemma 4.9. *Consider an initial condition $(r_1, \theta_1, \rho_1, \varepsilon_1)(0) = (r_1^*, \theta_1^*, R, \varepsilon_1^*) \in \Sigma_1^{\text{in}}$ for system (27). Then*

$$\begin{aligned} \theta_1(t_1) &= \theta_1^* + (R\varepsilon_1^*)^{\alpha-1} \varepsilon_1^{*-2} \left(1 - \left(1 - \frac{3}{2} \varepsilon_1^{*3} t_1 (1 + \mathcal{O}(R)) \right)^{2/3} \right) (1 + \mathcal{O}(R)) \pmod{1}, \\ \rho_1(t_1) &= R \left(1 - \frac{3}{2} \varepsilon_1^{*3} t_1 (1 + \mathcal{O}(R)) \right)^{\frac{1}{3}}, \\ \varepsilon_1(t_1) &= \varepsilon_1^* \left(1 - \frac{3}{2} \varepsilon_1^{*3} t_1 (1 + \mathcal{O}(R)) \right)^{-\frac{1}{3}}, \end{aligned}$$

for all $t_1 \in [0, T_1]$, where we use the notation $\mathcal{O}(R)$ to denote (possibly different) remainder terms which satisfy $|\mathcal{O}(R)| \leq CR$ for some constant $C > 0$ and all $t_1 \in [0, T_1]$. The transition time T_1 taken for the solution to reach Σ_1^{out} is given by

$$T_1 = \frac{2}{3} \left(\frac{1}{\varepsilon_1^{*3}} - \frac{1}{E^3} \right) (1 + \mathcal{O}(R)).$$

Proof. Consider system (27). By keeping track of the higher order terms when deriving the equation for ε_1' in system (27) one can show that

$$\varepsilon_1' = \frac{1}{2} \varepsilon_1^4 (1 - \rho_1 \chi(r_1, \theta_1, \rho_1, \varepsilon_1)),$$

where $\chi(r_1, \theta_1, \rho_1, \varepsilon_1) = \mathcal{O}(r_1, \rho_1, \varepsilon_1)$. Directly integrating and rearranging a little leads to

$$\varepsilon_1(t_1) = \varepsilon_1^* \left(1 - \frac{3}{2} \varepsilon_1^{*3} t_1 (1 + \psi(t_1)) \right)^{-\frac{1}{3}},$$

where

$$t_1 \psi(t_1) = - \int_0^{t_1} \rho_1(s_1) \chi(r_1(s_1), \theta_1(s_1), \rho_1(s_1), \varepsilon_1(s_1)) ds_1.$$

The expression for $\rho_1(t_1)$ can be obtained directly from the expression for $\varepsilon_1(t_1)$ using the fact that $\rho_1(t)\varepsilon_1(t) = \varepsilon = R\varepsilon_1^*$ is a constant of the motion; recall Remark 4.4. One can show that $|\psi(t_1)| = \mathcal{O}(R)$ by appealing to the fact that $\chi(r_1(s_1), \theta_1(s_1), \rho_1(s_1), \varepsilon_1(s_1))$ is bounded uniformly for all $s_1 \in [0, T_1]$, since $\rho_1 \in [0, R]$, $\varepsilon_1 \in [0, E]$, $\theta \in \mathbb{R}/\mathbb{Z}$ and $r_1 \in [-1 - \beta, -1 + \beta]$ (the latter follows from the fact that $r_1'|_{r_1=-1-\beta} > 0$ and $r_1'|_{r_1=-1+\beta} < 0$ if β is fixed sufficiently small). Therefore, there is a constant $C > 0$ such that $|\psi(t_1)| \leq CR$ for all $t_1 \in [0, T_1]$, as required.

It remains to estimate $\theta_1(t_1)$ and the transition time T_1 . We have that

$$\theta_1' = \rho_1(t_1)^{\alpha-1} \varepsilon_1(t_1)^\alpha \pmod{1} = (\varepsilon_1^* R)^{\alpha-1} \varepsilon_1(t_1) \pmod{1}.$$

The estimate for $\theta_1(t_1)$ is obtained via direct integration after substituting the expression for $\varepsilon_1(t_1)$. The estimate for T_1 is obtained using the equation for $\varepsilon_1(t_1)$ and the boundary constraint $\varepsilon_1(T_1) = E$ for T_1 ; c.f. [37, Lemma 2.7]. \square

Remark 4.10. *Dependent on the value of the parameter α , the time-scale of the rotational dynamics in chart K_1 is either fast, intermediate or slow with respect to $\varepsilon = R\varepsilon_1^* \rightarrow 0$. Specifically, solutions undergo*

$$N_{\text{rot},1}(\varepsilon_1^*, \alpha) = \lfloor \theta_1(T_1) - \theta_1(0) \rfloor = \left\lfloor (R\varepsilon_1^*)^{\alpha-1} \left(\frac{1}{\varepsilon_1^{*2}} - \frac{1}{E^2} \right) (1 + \mathcal{O}(R)) \right\rfloor$$

rotations as they traverse the neighbourhood between Σ_1^{in} and Σ_1^{out} , which is $\mathcal{O}(\varepsilon_1^{*-2})$ in case (C1)*, $\mathcal{O}(\varepsilon_1^{*\alpha-3})$ with $\alpha - 3 \in (-2, 0)$ in case (C1), $\mathcal{O}(1)$ in case (C2), and zero in case (C3).

Combining Lemmas 4.7 and 4.9 we obtain the following characterisation of the transition map $\Pi_1 : \Sigma_1^{\text{in}} \rightarrow \Sigma_1^{\text{out}}$, which summarises the dynamics in chart K_1 .

Proposition 4.11. *Fix $E, R, \beta > 0$ sufficiently small. Then the map $\Pi_1 : \Sigma_1^{\text{in}} \rightarrow \Sigma_1^{\text{out}}$ is well-defined and at least C^1 -smooth with the following properties:*

(a) (Asymptotics). *Let $c \in (0, 2)$ be the same constant as in Lemma 4.7. We have*

$$\Pi_1(r_1, \theta_1, R, \varepsilon_1) = \left(\Pi_{1,r_1}(r_1, \theta_1, \varepsilon_1), \theta_1 + (R\varepsilon_1)^{\alpha-1} \left(\frac{1}{\varepsilon_1^2} - \frac{1}{E^2} \right) (1 + \mathcal{O}(R)) \pmod{1}, \frac{R}{E} \varepsilon_1, E \right),$$

where

$$\Pi_{1,r_1}(r_1, \theta_1, \varepsilon_1) = h_{r_1} \left(\theta_1 + (R\varepsilon_1)^{\alpha-1} \left(\frac{1}{\varepsilon_1^2} - \frac{1}{E^2} \right) (1 + \mathcal{O}(R)), \frac{R}{E} \varepsilon_1, E \right) + \mathcal{O} \left(e^{-2c/3\varepsilon_1^3} \right).$$

The function h_{r_1} is described by Lemma 4.7.

(b) (Strong contraction). *The r_1 -component of Π_1 is a strong contraction with respect to r_1 . More precisely,*

$$\frac{\partial \Pi_{1,r_1}}{\partial r_1}(r_1, \theta_1, \varepsilon_1) = \mathcal{O} \left(e^{-2c/3\varepsilon_1^3} \right).$$

The image $\Pi_1(\Sigma_1^{\text{in}}) \subset \Sigma_1^{\text{out}}$ is a wedge-like region about the intersection $M_1^{\text{a}} \cap \Sigma_1^{\text{out}}$.

Proof. Consider an initial condition $(r_1, \theta_1, R, \varepsilon_1) \in \Sigma_1^{\text{in}}$. The form of the map $\Pi_1(r_1, \theta_1, R, \varepsilon_1)$ follows immediately after evaluating the solutions for $\theta_1(t_1), \rho_1(t_1)$, and $\varepsilon_1(t_1)$ at $t_1 = T_1$ using Lemma 4.9. The expression for $r_1(T_1) = \Pi_{1,r_1}(r_1, \theta_1, \varepsilon_1)$ follows from Lemma 4.7. Specifically, choosing $E, R, \beta > 0$ sufficiently small ensures that the initial condition $(r_1, \theta_1, R, \varepsilon_1)$ is contained in a fast fiber of M_1^{a} . It follows that

$$\|r_1(T_1) - h_{r_1}(\theta_1(T_1), \rho_1(T_1), E)\| = \mathcal{O}(e^{-cT_1})$$

for a constant $c \in (0, 2)$. Thus $r_1(T_1) = h_{r_1}(\theta_1(T_1), \rho_1(T_1), E) + \mathcal{O}(e^{-cT_1})$, which yields the expression in Assertion (a) after substituting the expression for T_1 in Lemma 4.9.

Assertion (b) follows by direct differentiation. The estimate follows since $h_{r_1}(\theta_1, \rho_1, \varepsilon_1)$ does not depend on r_1 . \square

Remark 4.12. *Strictly speaking, the arguments above only guarantee that Π_1 is well-defined for initial conditions with $\varepsilon_1 \in (0, E]$. This is not problematic since we aim to derive results for $\varepsilon > 0$.*

4.3 Dynamics in the rescaling chart K_2

In chart K_2 we study solutions close to the extension of the center manifold $M_2^a = \kappa_{12}(M_1^a)$.

Lemma 4.13. *Following the singular time rescaling $\rho_2 dt = dt_2$ or equivalently, $\rho_2 t = t_2$, the desingularized equations in chart K_2 are given by*

$$\begin{aligned} r_2' &= -y_2 + r_2^2 + \mathcal{O}(\rho_2), \\ \theta_2' &= \rho_2^{\alpha-1}, \\ y_2' &= -1 + \mathcal{O}(\rho_2), \\ \rho_2' &= 0, \end{aligned} \tag{31}$$

where by a slight abuse of notation we now write $(\cdot)' = d/dt_2$. Since $0 < \rho_2 = \varepsilon \ll 1$, system (31) can also be viewed as a perturbation problem in (r_2, θ_2, y_2) -space as $\rho_2 \rightarrow 0$.

Proof. This follows immediately after differentiating the defining expressions for local K_2 coordinates in (25) and applying $\rho_2 t = t_2$. \square

The key observation is that the angular variable completely decouples in the limit as $\rho_2 \rightarrow 0$, i.e. in the system

$$\begin{aligned} r_2' &= -y_2 + r_2^2, \\ \theta_2' &= 0^{\alpha-1}, \\ y_2' &= -1. \end{aligned} \tag{32}$$

There are two possibilities for the angular dynamics, depending on α , since

$$\theta_2' = \begin{cases} 1, & \alpha = 1, \\ 0, & \alpha > 1. \end{cases}$$

In either case, the planar system

$$\begin{aligned} r_2' &= -y_2 + r_2^2, \\ y_2' &= -1, \end{aligned} \tag{33}$$

decouples. System (33) is precisely the Riccati-type equation which arises within the K_2 chart in the analysis of the regular fold point in [37]. Solutions to system (33) can be written in terms of Airy functions, whose asymptotic properties are known [18, 46]. The properties that are relevant for our purposes are collected in [46] and reformulated in a notation similar to ours in [37]. The following result is a direct extension of the latter formulation; we simply append the existing result with the decoupled angular dynamics induced by the equation for θ .

Proposition 4.14. *Consider the restricted system (31)| $_{\rho_2=0}$ or, equivalently, the limiting system (32). The following assertions are true:*

- (a) *Every orbit approaches the two-dimensional horizontal asymptote/plane $y_2 = y_r$ from $y_2 > y_r$ as $r_2 \rightarrow \infty$. The value of y_r depends on the initial conditions.*
- (b) *There exists a unique, invariant two-dimensional surface*

$$\gamma_2 := \{(r_2, \theta_2, h_{y_2}(r_2), 0) : r_2 \in \mathbb{R}, \theta_2 \in \mathbb{R}/\mathbb{Z}\}, \tag{34}$$

where $h_{y_2}(r_2)$ is smooth with asymptotics

$$\begin{aligned} h_{y_2}(r_2) &= r_2^2 + \frac{1}{2r_2} + \mathcal{O}\left(\frac{1}{r_2^4}\right) && \text{as } r_2 \rightarrow -\infty, \\ h_{y_2}(r_2) &= -\Omega_0 + \frac{1}{r_2} + \mathcal{O}\left(\frac{1}{r_2^3}\right) && \text{as } r_2 \rightarrow \infty, \end{aligned}$$

and Ω_0 is the constant defined in Theorem 3.2.

- (c) All orbits with initial conditions to the right of γ_2 in the (r_2, y_2) -plane are backwards asymptotic to the paraboloid $\{(r_2, \theta_2, r_2^2, 0) : r_2 \geq 0, \theta_2 \in \mathbb{R}/\mathbb{Z}\}$.
- (d) All orbits with initial condition to the left of γ_2 in the (r_2, y_2) -plane are backwards asymptotic to a horizontal asymptote/plane $y_2 = y_l$. Specifically, $y_2(t_2) \rightarrow y_l$ from below and $r_2(t_2) \rightarrow -\infty$ as $t_2 \rightarrow -\infty$. The value of y_l depends on the initial conditions, but satisfies $y_l > y_r$ for each fixed orbit.
- (e) The unique center manifold N_1^a described in Lemma 4.7 coincides with the surface γ_2 where K_1 and K_2 overlap, i.e. $\kappa_{12}(N_1^a) = \gamma_2$ on $\{y_2 > 0\}$.

Proof. See [46] and in particular [37, Prop. 2.3], which cover Assertions (a)-(d) in planar case, i.e. for system (33). Since the angular dynamics in θ decouples from system (32), Assertions (a)-(d) are obtained as higher dimensional analogues from these results after a simple rotation through $\theta_2 \in [0, 1)$.

Assertion (e) is a straightforward adaptation of [37, Prop. 2.6 Assertion (5)]. \square

The Riccati dynamics described in Proposition 4.14 are sketched for the decoupled planar system (33) in Figure 12, and for the three-dimensional limiting system (32) in Figure 13. Proposition 4.14 can be used to describe the limiting behaviour of the y_2 -component of the map $\Pi_2 : \Sigma_2^{\text{in}} \rightarrow \Sigma_2^{\text{out}}$ induced by the flow of initial conditions in

$$\Sigma_2^{\text{in}} := \{(r_2, \theta_2, E^{-2}, \rho_2) : |r_2 + E^{-1}| \leq \beta E^{-1}, \theta_2 \in \mathbb{R}/\mathbb{Z}, \rho_2 \in [0, ER]\},$$

which is related to the exit section in chart K_1 via $\Sigma_2^{\text{in}} = \kappa_{12}(\Sigma_1^{\text{out}})$, up to the exit section

$$\Sigma_2^{\text{out}} := \{(E^{-1}, \theta_2, y_2, \rho_2) : \theta_2 \in \mathbb{R}/\mathbb{Z}, y_2 \in [-\nu E^{-2}, \nu E^2], \rho_2 \in [0, ER]\},$$

where $\nu > 0$ is small but fixed.

Similarly to the analysis in K_1 , the remaining components of the image $\Pi_2(r_2, \theta_2, E^{-2}, \rho_2)$ and the transition time T_2 taken for initial conditions in Σ_2^{in} to reach Σ_2^{out} can be calculated directly.

Lemma 4.15. *Consider an initial condition $(r_2, \theta_2, E^{-2}, \rho_2)(0) = (r_2^*, \theta_2^*, E^{-2}, \rho_2) \in \Sigma_2^{\text{in}}$ for system (31). Then*

$$\begin{aligned} \theta_2(t_2) &= \theta_2^* + \rho_2^{\alpha-1} t_2 \pmod{1}, \\ y_2(t_2) &= y_2^* + t_2(-1 + \mathcal{O}(\rho_2)). \end{aligned}$$

Proof. The solutions are obtained by direct integration. \square

Combining Proposition 4.14 and Lemma 4.15, we obtain the following characterisation of the transition map $\Pi_2 : \Sigma_2^{\text{in}} \rightarrow \Sigma_2^{\text{out}}$, which summarises the dynamics in chart K_2 .

Proposition 4.16. *Fix $E, R, \beta > 0$ sufficiently small. Then the map $\Pi_2 : \Sigma_2^{\text{in}} \rightarrow \Sigma_2^{\text{out}}$ is a well-defined diffeomorphism with asymptotics*

$$\begin{aligned} \Pi_2(r_2, \theta_2, E^{-2}, \rho_2) &= \\ & (E^{-1}, \theta_2 + \rho_2^{\alpha-1} (E^{-2} - h_{y_2}(E^{-1}) + \mathcal{O}(r_2 - r_{2,c}, \rho_2)) \pmod{1}, h_{y_2}(E^{-1}) + \mathcal{O}(r_2 - r_{2,c}, \rho_2), \rho_2), \end{aligned}$$

where $h_{y_2}(r_2)$ is the Riccati function which defines the surface γ_2 in (34) and $r_{2,c}$ is the (unique) r_2 -coordinate of the intersection $\gamma_2 \cap \Sigma_2^{\text{in}}$, which is defined implicitly via the relation $h_{y_2}(r_{2,c}) = E^{-2}$.

Proof. Let $(r_{2,c}, \theta_2, E^{-2}, 0)$ denote the K_2 coordinates of the intersection $\gamma_2 \cap \Sigma_2^{\text{in}}$. It follows from Proposition 4.14 and Lemma 4.15 that

$$\Pi_2(r_{2,c}, \theta_2, E^{-2}, 0) = (E^{-1}, \theta_2 + \rho_2^{\alpha-1} T_2 \pmod{1}, h_{y_2}(E^{-1}), 0) \in \text{Int } \Sigma_2^{\text{out}},$$

where $T_2 > 0$ is the time taken to reach Σ_2^{out} , $\text{Int } \Sigma_2^{\text{out}}$ denotes the interior of Σ_2^{out} in $\{E^{-1}\} \times \mathbb{R}/\mathbb{Z} \times \mathbb{R} \times \mathbb{R}_{\geq 0}$, and the containment in $\text{Int } \Sigma_2^{\text{out}}$ follows from the asymptotics $h_{y_2}(\eta^{-1}) = -\Omega_0 + \eta + \mathcal{O}(\eta^3)$ as

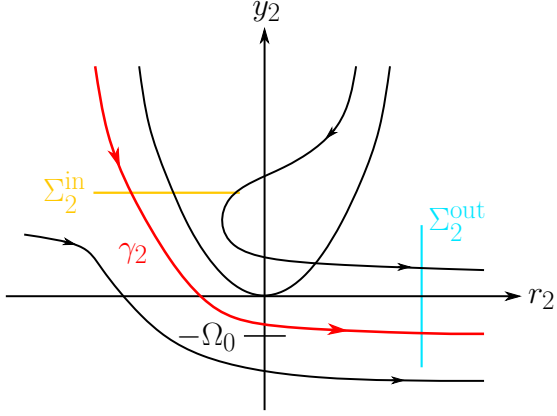


Figure 12: Dynamics for the Riccati equation (33) in the (r_2, y_2) -plane. The distinguished solution γ_2 with asymptotics described by Proposition 4.14 and [37, Prop. 2.3] is shown in red. The parabola $y_2 = r_2^2$ which separates solutions with different asymptotic properties is also shown. Projections of the entry and exit sections Σ_2^{in} and Σ_2^{out} are shown in yellow and cyan respectively.

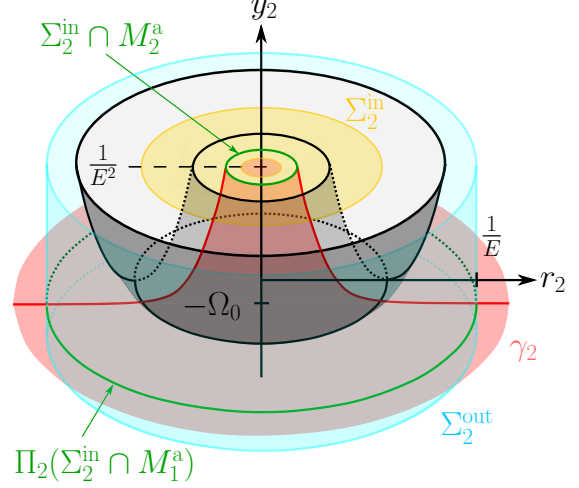


Figure 13: Geometry and dynamics of the limiting Riccati equation (31) $_{|\rho_2=0}$ (or equivalently (32)) in (r_2, θ_2, y_2) -space. The two-dimensional surface γ_2 is shown in shaded red, and coincides with the extension of the two-dimensional center manifold N_1^a described in Lemma 4.7 into chart K_2 according to Proposition 4.14 Assertion (e). The evolution of initial conditions in Σ_2^a up to Σ_2^{out} is described by Proposition 4.16, which implies that the image $\Pi_2(\gamma_2 \cap \Sigma_1^a) \subset \Sigma_2^{\text{out}}$, shown here in green, is a circle contained within the constant plane $\{y_2 = -\Omega_0 + E\}$ (see also Lemma 4.18).

$\eta \rightarrow 0^+$ in Proposition 4.14 Assertion (b). The transition time can be estimated using Lemma 4.15. In particular,

$$y_2(T_2) = h_{y_2}(E^{-1}) = y_2(0) - T_2 = E^{-2} - T_2 \quad \Rightarrow \quad T_2 = E^{-2} - h_{y_2}(E^{-1}),$$

which implies that

$$\Pi_2(r_{2,c}, \theta_2, E^{-2}, 0) = (E^{-1}, \theta_2 + \rho_2^{\alpha-1} (E^{-2} - h_{y_2}(E^{-1})) \bmod 1, h_{y_2}(E^{-1}), 0). \quad (35)$$

Since the transition time T_2 is finite and system (32) is a regular perturbation problem, a neighbourhood of $(r_{2,c}, \theta_2, E^{-2}, 0) \in \Sigma_2^{\text{in}}$ is mapped diffeomorphically to a neighbourhood of $\gamma_2 \cap \Sigma_2^{\text{out}}$ in Σ_2^{out} . The form of the map in Proposition 4.16 follows. \square

The extension of M_2^a up to Σ_2^{out} , as described by Proposition 4.16, is shown in projections onto (r_2, θ_2, y_2) - and (r_2, y_2, ρ_2) -space in Figures 13 and 14 respectively.

Remark 4.17. Proposition 4.16 shows that solutions undergo a total of

$$N_{\text{rot},2}(\rho_2, \alpha) = \lfloor \theta_2(T_2) - \theta_2(0) \rfloor = \lfloor \rho_2^{\alpha-1} (E^{-2} - h_{y_2}(E^{-1}) + \mathcal{O}(r_2 - r_{2,c}, \rho_2)) \rfloor$$

rotations as they traverse the neighbourhood between Σ_2^{in} and Σ_2^{out} . Thus, the number of rotations in chart K_2 is $\mathcal{O}(1)$ if $\alpha = 1$ (i.e. in case (C1)*), but zero for all $\alpha > 1$ (i.e. in all other cases (C1), (C2) and (C3)).

Finally we note that the expression for $h_{y_2}(E^{-1})$ (and therefore the map Π_2) can be simplified using the following result, which can be found in [37].

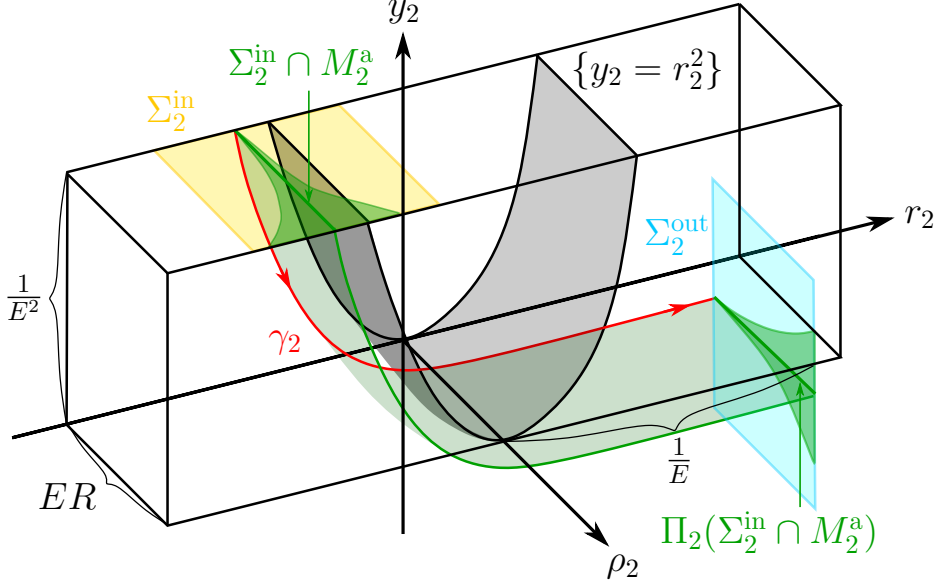


Figure 14: Geometry and dynamics projected into (r_2, y_2, ρ_2) -space; c.f. Figures 12 and 13. The extension of the (projected) three-dimensional manifold M_2^a is sketched in shaded green. The image of the wedge-shaped region $\kappa_{12}(\Pi_1(\Sigma_1^{\text{in}})) \subset \Sigma_2^{\text{in}}$ (recall Proposition 4.11) under Π_2 is also shown in shaded green.

Lemma 4.18. *The Riccati function h_{y_2} defined in Proposition 4.14 satisfies*

$$h_{y_2}(E^{-1}) = -\Omega_0 + E.$$

Proof. This can be proven using the asymptotic properties of the decoupled Riccati equation (33) described in Proposition 4.14. Since the proof does not depend on the angular dynamics, we refer to [37, Rem. 2.10 and Prop. 2.11]. \square

4.4 Dynamics in the exit chart K_3

In chart K_3 we study solutions close to the extension of the manifold $M_3^a = \kappa_{23}(M_2^a)$ as it leaves a neighbourhood of the singular cycle S_0^c .

Lemma 4.19. *Following the positive transformation of time $\rho_3 dt = dt_3$, the desingularized equations in chart K_3 are given by*

$$\begin{aligned} \rho_3' &= \rho_3 F(\rho_3, \theta_3, y_3, \varepsilon_3), \\ \theta_3' &= \rho_3^{\alpha-1} \varepsilon_3^\alpha, \\ y_3' &= -2y_3 F(\rho_3, \theta_3, y_3, \varepsilon_3) + \varepsilon_3^3(-1 + \mathcal{O}(\rho_3)), \\ \varepsilon_3' &= -\varepsilon_3 F(\rho_3, \theta_3, y_3, \varepsilon_3), \end{aligned} \tag{36}$$

where $F(\rho_3, \theta_3, y_3, \varepsilon_3) = 1 - y_3 + \mathcal{O}(\rho_3)$.

Proof. This follows after direct differentiation of the local coordinate expressions in (25) and subsequent application of the desingularization $\rho_3 dt = dt_3$. \square

Except for the angular coordinate θ_3 , the analysis in K_3 is entirely local. Specifically, we focus on dynamics within the set

$$\mathcal{D}_3 := \{(\rho_3, \theta_3, y_3, \varepsilon_3) : \rho_3 \in [0, R], \theta_3 \in \mathbb{R}/\mathbb{Z}, y_3 \in [-\nu, \nu], \varepsilon_3 \in [0, E]\},$$

where E , R and ν are the same positive constants used to define the entry and exit sections in charts K_1 and K_2 . System (36) has a circular critical manifold

$$Q := \{(0, \theta_3, 0, 0) : \theta_3 \in \mathbb{R}/\mathbb{Z}\},$$

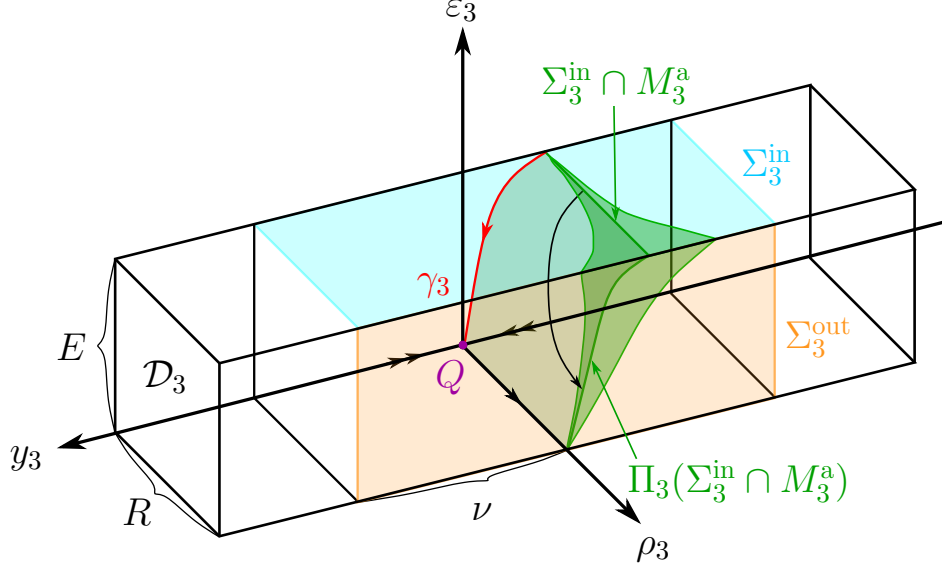


Figure 15: Geometry and dynamics within \mathcal{D}_3 , shown in $(r_3, \rho_3, \varepsilon_3)$ -space. The (projection of the) two-dimensional surface $\gamma_3 = \kappa_{23}(\gamma_2)$ shown in red connects to the circular saddle-type critical manifold Q , which is indicated by the purple dot at the origin. Entry and exit sections Σ_3^{in} and Σ_3^{out} are shown in shaded cyan and orange respectively. The wedge-shaped region within Σ_2^{out} (shown in shaded green in Figure 14) is shown here in Σ_3^{in} (again in shaded green), along with its image in Σ_3^{out} under Π_3 . The projection of the three-dimensional manifold M_3^a with base along $\gamma_3 \cup \{y_3 = \varepsilon_3 = 0, \rho_3 \geq 0\}$ is also shown.

with the following properties.

Lemma 4.20. *Consider system (36). Q is normally hyperbolic and saddle-type. More precisely, the linearization along Q has eigenvalues*

$$\lambda_1 = 1, \quad \lambda_2 = 0, \quad \lambda_3 = -2, \quad \lambda_4 = -1,$$

and corresponding eigenvectors $(1, 0, 0, 0)$, $(0, 1, 0, 0)$, $(0, 0, 1, 0)$ and $(0, 0, 0, 1)$ respectively.

Proof. Direct calculation. □

Lemma 4.20 implies the existence of local center, stable and unstable center manifolds at Q . Specifically, there is a one-dimensional center manifold $W_3^c(Q)$, a two-dimensional stable manifold $W_3^s(Q)$, and a one-dimensional unstable manifold $W_3^u(Q)$. The geometry is sketched in different three-dimensional subspaces and projections in Figures 15, 16 and 17.

We now show that the extension of the surface γ_2 connects to the critical manifold Q tangentially to the cylinder spanned by the center and weakly stable eigenvectors.

Lemma 4.21. *The extension of γ_2 under system (36), i.e. $\gamma_3 = \kappa_{23}(\gamma_2)$, connects to Q tangentially to the cylinder segment $\{(0, \theta_3, 0, \varepsilon_3) \in \mathcal{D}_3\}$.*

Proof. Applying the change of coordinates formula in (26) together with the Riccati asymptotics as $r_2 \rightarrow \infty$ in Proposition 4.14 Assertion (b), we obtain

$$\kappa_{23}(\gamma_2) \cap \mathcal{D}_3 = \{(0, \theta_3, \varepsilon_3^2(-\Omega_0 + \varepsilon_3 + \mathcal{O}(\varepsilon_3^3)), \varepsilon_3) : \theta_3 \in \mathbb{R}/\mathbb{Z}, \varepsilon_3 \in [0, E]\},$$

which converges to the critical manifold Q tangentially to $\{(0, \theta_3, 0, \varepsilon_3) \in \mathcal{D}_3\}$ as $\varepsilon_3 \rightarrow 0$. □

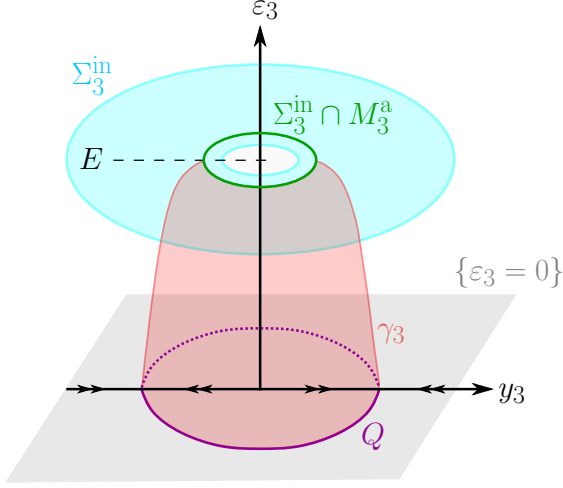


Figure 16: Geometry and dynamics within the invariant hyperplane $\{\rho_3 = 0\}$, projected into $(y_3, \theta_3, \varepsilon_3)$ -space; c.f. Figure 15.

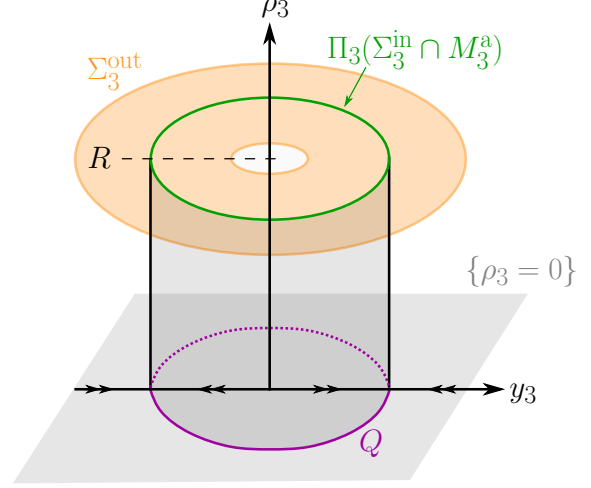


Figure 17: Geometry and dynamics within the invariant hyperplane $\{\varepsilon_3 = 0\}$, projected into (y_3, θ_3, ρ_3) -space; c.f. Figures 15 and 16.

Having described the geometry, we turn our attention to the characteristics of the map $\Pi_3 : \Sigma_3^{\text{in}} \rightarrow \Sigma_3^{\text{out}}$ induced by the flow of initial conditions in

$$\Sigma_3^{\text{in}} := \{(\rho_3, \theta_3, y_3, E) \in \mathcal{D}_3\},$$

which corresponds to the exit section Σ_2^{out} in chart K_2 via $\Sigma_3^{\text{in}} = \kappa_{23}(\Sigma_2^{\text{out}})$, up to the exit section

$$\Sigma_3^{\text{out}} := \{(R, \theta_3, y_3, \varepsilon_3) \in \mathcal{D}_3\},$$

which is precisely the representation of the exit section $\Delta_\varepsilon^{\text{out}}$ defined in (23) after blow-up in chart K_3 if we set $y_0 = R^2\nu$. Similarly to the K_3 analysis for the regular fold point in [37], Π_3 can be analysed directly after a second positive transformation of time $F(\rho_3, \theta_3, y_3, \varepsilon_3)dt_3 = d\tilde{t}_3$, which amounts to division of the right-hand side in system (36) by $F(\rho_3, \theta_3, y_3, \varepsilon_3)$ (which is strictly positive in \mathcal{D}_3). This leads to the orbitally equivalent system

$$\begin{aligned} \rho_3' &= \rho_3, \\ \theta_3' &= \frac{\rho_3^{\alpha-1}\varepsilon_3^\alpha}{1-y_3+\mathcal{O}(\rho_3)} = \rho_3^{\alpha-1}\varepsilon_3^\alpha + \mathcal{O}(\rho_3^{\alpha-1}\varepsilon_3^\alpha y_3, \rho_3^\alpha \varepsilon_3^\alpha), \\ y_3' &= -2y_3 + \frac{\varepsilon_3^3(-1+\mathcal{O}(\rho_3))}{1-y_3+\mathcal{O}(\rho_3)} = -2y_3 - \varepsilon_3^3 + \mathcal{O}(\varepsilon_3^3 y_3, \rho_3 \varepsilon_3^3), \\ \varepsilon_3' &= -\varepsilon_3, \end{aligned} \tag{37}$$

where by a slight abuse of notation the prime notation now refers to differentiation with respect to \tilde{t}_3 .

System (37) is used to obtain the following result.

Proposition 4.22. *Fix $E, R, \nu > 0$ sufficiently small. Then the map $\Pi_3 : \Sigma_3^{\text{in}} \rightarrow \Sigma_3^{\text{out}}$ is well-defined, at least C^1 -smooth and given by*

$$\Pi_3(\rho_3, \theta_3, y_3, E) = \left(R, \theta_3 + \rho_3^{\alpha-1} E^\alpha \left(1 - \frac{\rho_3}{R}\right) + \mathcal{O}\left(\rho_3^\alpha \ln\left(\frac{1}{\rho_3}\right)\right) \bmod 1, h_{y_3}(\rho_3, \theta_3, y_3), \frac{E}{R}\rho_3 \right),$$

where

$$h_{y_3}(\rho_3, \theta_3, y_3) = (y_3 - E^3) \left(\frac{\rho_3}{R}\right)^2 + \mathcal{O}\left(\rho_3^3 \ln\left(\frac{1}{\rho_3}\right)\right).$$

Proof. The proof proceeds similarly the proof of [37, Prop. 2.11], except that we need to account for the angular dynamics in θ_3 .

We consider solutions of system (37) which satisfy $(\rho_3, \theta_3, y_3, \varepsilon_3)(0) = (\rho_3^*, \theta_3^*, y_3^*, E) \in \Sigma_3^{\text{in}}$ and $(R, \theta_3, y_3, \varepsilon_3)(T_3) \in \Sigma_3^{\text{out}}$ for some $T_3 > 0$. The equations for ρ_3 and ε_3 can be solved directly, leading to $\rho_3(t_3) = \rho_3^* e^{t_3}$ and $\varepsilon_3(t_3) = E e^{-t_3}$, and the boundary constraint $\rho_3(T_3) = R$ leads to the following expression for the transition time:

$$T_3 = \ln \left(\frac{R}{\rho_3^*} \right).$$

It follows that $\varepsilon_3(T_3) = E \rho_3^*/R$, as required. We need to estimate $y_3(T_3)$ and $\theta_3(T_3)$ at $t_3 = T_3$. Substituting the solutions for $\rho_3(\tilde{t}_3)$ and $\varepsilon_3(\tilde{t}_3)$ into the equations for θ_3 and y_3 in system (37) leads to the planar non-autonomous system

$$\begin{aligned} \theta_3' &= \rho_3^{*\alpha-1} E^\alpha e^{-\tilde{t}_3} + \rho_3^{*\alpha-1} \mathcal{O}(y_3 e^{-\tilde{t}_3}, \rho_3^*), \\ y_3' &= -2y_3 - E^3 e^{-3\tilde{t}_3} + e^{-2\tilde{t}_3} \mathcal{O}(y_3 e^{-\tilde{t}_3}, \rho_3^*). \end{aligned}$$

Notice that for sufficiently small E we have $y_3'|_{y_3=-\nu} > 0$ and $y_3'|_{y_3=\nu} < 0$. It follows that Π_3 is well-defined, since solutions are inflowing along the faces of \mathcal{D}_3 defined by $\{y = \pm\nu\}$ for all $\tilde{t}_3 \in [0, T_3]$.

In order to estimate $y_3(T_3)$, we introduce a new time-dependent variable z_3 via

$$y_3(\tilde{t}_3) = (y_3^* - E^3 + z_3(\tilde{t}_3)) e^{-2\tilde{t}_3} + E^3 e^{-3\tilde{t}_3}.$$

Differentiating $y_3(\tilde{t}_3)$ and using $\rho_3(\tilde{t}_3) = \rho_3^* e^{\tilde{t}_3}$ leads to the following ODE in z_3 :

$$z_3' = \mathcal{O}(y_3 e^{-\tilde{t}_3}, \rho_3^*) = \mathcal{O} \left(\frac{y_3 \rho_3^*}{\rho_3}, \rho_3^* \right),$$

with initial condition $z_3(0) = 0$. Since $|y_3(\tilde{t}_3)| \leq \nu$ and $|\rho_3(\tilde{t}_3)| \geq \rho_3^*$ for all $\tilde{t}_3 \in [0, T_3]$, we have that

$$z_3' \in \mathcal{O}(\rho_3^*) \quad \Rightarrow \quad z_3(\tilde{t}_3) \in \mathcal{O}(\rho_3^* \tilde{t}_3) \quad \Rightarrow \quad z_3(T_3) \in \mathcal{O}(\rho_3^* T_3) = \mathcal{O} \left(\rho_3^* \ln \left(\frac{1}{\rho_3^*} \right) \right).$$

Changing variables back to y_3 and evaluating at $\tilde{t}_3 = T_3$ yields

$$y_3(T_3) = (y_3^* - E^3 + z_3(T_3)) e^{-2T_3} + E^3 e^{-3T_3} = (y_3^* - E^3) \left(\frac{\rho_3^*}{R} \right)^2 + \mathcal{O} \left((\rho_3^*)^3 \ln \left(\frac{1}{\rho_3^*} \right) \right),$$

as required.

It remains to estimate $\theta_3(T_3)$. This can be done using arguments similar to those used to estimate $y_3(T_3)$ above. We define a new variable z_θ via

$$\theta_3(\tilde{t}_3) = \theta_3^* + (\rho_3^* E)^{\alpha-1} \left(E - E e^{-\tilde{t}_3} \right) + z_\theta(\tilde{t}_3),$$

and differentiate in order to obtain the following equation for z_θ :

$$z_\theta' = \mathcal{O}(\rho_3^{*\alpha-1} y_3 e^{-\tilde{t}_3}, \rho_3^{*\alpha}) = \mathcal{O} \left(\frac{y_3 \rho_3^{*\alpha}}{\rho_3}, \rho_3^{*\alpha} \right),$$

with initial condition $z_\theta(0) = 0$. Using the same arguments as for the ODE for z_3 we obtain

$$z_\theta' \in \mathcal{O}(\rho_3^{*\alpha}) \quad \Rightarrow \quad z_\theta(\tilde{t}_3) \in \mathcal{O}(\rho_3^{*\alpha} \tilde{t}_3) \quad \Rightarrow \quad z_\theta(T_3) \in \mathcal{O}(\rho_3^{*\alpha} T_3) = \mathcal{O} \left(\rho_3^{*\alpha} \ln \left(\frac{1}{\rho_3^*} \right) \right).$$

Changing variables back to θ_3 and evaluating at $\tilde{t}_3 = T_3$ leads to

$$\theta_3(T_3) = \theta_3^* + (\rho_3^* E)^{\alpha-1} \left(E - E \frac{\rho_3^*}{R} \right) + \mathcal{O} \left(\rho_3^{*\alpha} \ln \left(\frac{1}{\rho_3^*} \right) \right),$$

as required. □

Note that systems (36) and (37) are orbitally equivalent. Since the result in Proposition 4.22 only depends on the initial condition in Σ_3^{in} , and not on the transition time, it holds for both systems (36) and (37).

Remark 4.23. *Similarly to the arguments used to describe the map Π_1 in proof of Proposition 4.11, the arguments used to describe the map Π_3 in Proposition 4.22 are (strictly speaking) only valid for initial conditions with $\rho_3 \in (0, R]$. This is not problematic since we aim to derive results for $\varepsilon > 0$. Moreover, Π_3 can be smoothly and uniquely extended to $\rho_3 = 0$ by defining $\Pi_3(0, \theta_3, y_3, E) = (R, \theta_3 + \rho_3^{\alpha-1} E^\alpha \bmod 1, 0, 0)$.*

Remark 4.24. *Proposition 4.22 shows that the rotation in chart K_3 is slow for all $\alpha \geq 1$ and therefore for all cases $(C1)^*$, $(C1)$, $(C2)$ and $(C3)$. In particular, solutions undergo*

$$N_{\text{rot},3}(\varepsilon_3^*, \alpha) = \lfloor \theta_3(T_3) - \theta_3(0) \rfloor = 0$$

rotations as they traverse the neighbourhood from Σ_3^{in} to Σ_3^{out} .

4.5 Proof of Theorem 3.2

We now combine the results obtained in the charts K_1 , K_2 and K_3 in order to prove the Theorem 3.2. The idea is to describe the extended map $\pi_\varepsilon : \Delta_\varepsilon^{\text{in}} \rightarrow \Delta_\varepsilon^{\text{out}}$ defined in Section 4.1, the first three components of which coincide with components of $\pi : \Delta^{\text{in}} \rightarrow \Delta^{\text{out}}$, via its preimage in the blown-up space:

$$\Pi := \Pi_3 \circ \kappa_{23} \circ \Pi_2 \circ \kappa_{12} \circ \Pi_1 : \Sigma_1^{\text{in}} \rightarrow \Sigma_3^{\text{out}}.$$

This can be done explicitly using the change of coordinate maps κ_{ij} in Lemma 4.1 and the characterisation of Π_1 , Π_2 and Π_3 in Propositions 4.11, 4.16 and 4.22 respectively. Note that these results immediately imply that Π is at least C^1 -smooth, since each κ_{ij} and Π_i is at least C^1 -smooth. The geometry is sketched in Figure 18.

We now derive the form of the map Π . Initial conditions $(r_1, \theta_1, R, \varepsilon_1) \in \Sigma_1^{\text{in}}$ are mapped to Σ_1^{out} under Π_1 as described by Proposition 4.11. Since $\Sigma_2^{\text{in}} = \kappa_{12}(\Sigma_1^{\text{out}})$, we obtain the following input for the map Π_2 :

$$\begin{aligned} (r_2, \theta_2, y_2, \rho_2) &= \kappa_{12}(\Pi_1(r_1, \theta_1, R, \varepsilon_1)) \\ &= \left(\frac{h_{r_1}(\theta_1, \rho_1, \varepsilon_1)}{E}, \theta_1 + (R\varepsilon_1)^{\alpha-1} \left(\frac{1}{\varepsilon_1^2} - \frac{1}{E^2} \right) (1 + \mathcal{O}(R)) \bmod 1, \frac{1}{E^2}, R\varepsilon_1 \right). \end{aligned} \quad (38)$$

Before substituting these values into the expression for Π_2 in Proposition 4.16, notice that the strong contraction property in Proposition 4.11(b) implies the initial conditions in (38) satisfy

$$r_2 - r_{2,c} = \frac{1}{E} (h_{r_1}(\theta_1, \rho_1, \varepsilon_1) - r_{1,c}) = \mathcal{O} \left(e^{-2c/3\varepsilon_1^3} \right),$$

where $c \in (0, 2)$ is a constant and $r_{1,c}$ denotes the (unique) r_1 -value of the intersection $N_1^a \cap \Sigma_1^{\text{out}}$ (see also Proposition 4.14(e)). Using this together with the formula for $h_{y_2}(E^{-1})$ in Lemma 4.18, equation (38), Lemma 4.1 and Proposition 4.16, we obtain an expression for the input to the map Π_3 , namely

$$\begin{aligned} (\rho_3, \theta_3, y_3, \varepsilon_3) &= \kappa_{23}(\Pi_2(r_2, \theta_2, y_2, \rho_2)) \\ &= \left(\frac{R}{E} \varepsilon_1, \theta_1 + (R\varepsilon_1)^{\alpha-1} \left(\frac{1}{\varepsilon_1^2} + \Omega_0 - E \right) (1 + \mathcal{O}(R)) \bmod 1, -E^2 \Omega_0 + E^3 + \mathcal{O}(\varepsilon_1), E \right). \end{aligned} \quad (39)$$

Substituting the right-most expression in (39) into the expression for $\Pi_3(\rho_3, \theta_3, y_3, E)$ in Proposition 4.22 yields an expression for $\Pi(r_1, \theta_1, R, \varepsilon_1)$. We obtain

$$\begin{aligned} \Pi(r_1, \theta_1, R, \varepsilon_1) &= \\ &= \left(R, \theta_1 + (R\varepsilon_1)^{\alpha-1} \left(\frac{1}{\varepsilon_1^2} + \Omega_0 \right) (1 + \mathcal{O}(R)) + \mathcal{O} \left(\varepsilon_1^\alpha \ln \frac{1}{\varepsilon_1} \right) \bmod 1, -\Omega_0 \varepsilon_1^2 + \mathcal{O} \left(\varepsilon_1^3 \ln \frac{1}{\varepsilon_1} \right), \varepsilon_1 \right). \end{aligned} \quad (40)$$

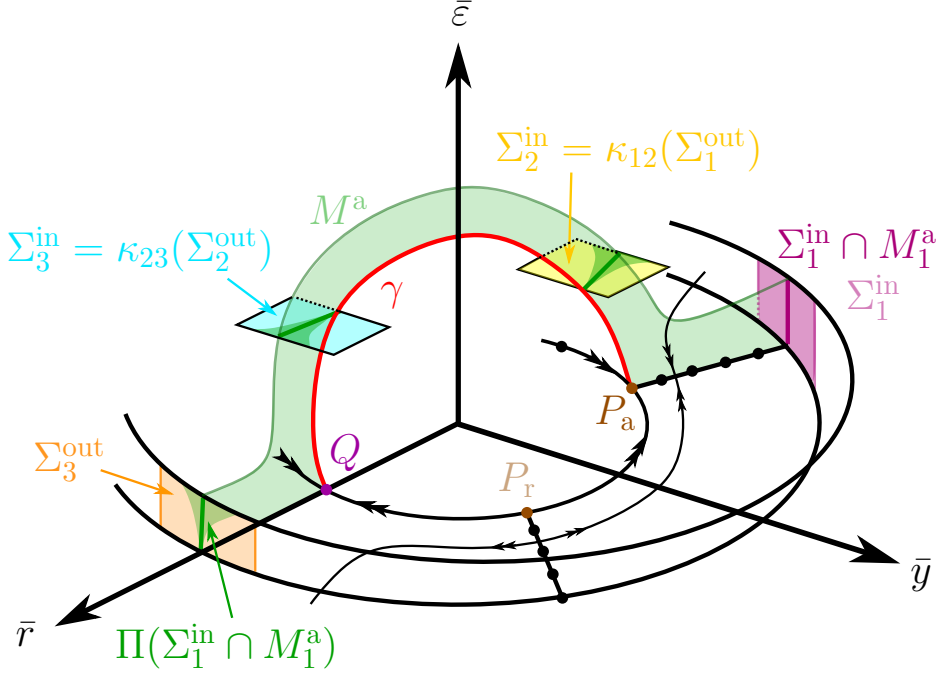


Figure 18: Global geometry and dynamics in the blown-up space projected into $(\bar{r}, \bar{y}, \bar{\varepsilon})$ -space. The three-dimensional manifold M^a which extends from $\Delta_\varepsilon^{\text{in}}$ up to $\Delta_\varepsilon^{\text{out}}$ (which are identified with Σ_1^{in} and Σ_3^{out} respectively) is shown again in shaded green. Theorem 3.2 is proven by combining results obtained in charts K_1 , K_2 and K_3 : The flow from Σ_1^{in} to Σ_1^{out} is described by Proposition 4.11, the flow from Σ_2^{in} to Σ_2^{out} is described by Proposition 4.16 and the flow from Σ_3^{in} to Σ_3^{out} is described by Proposition 4.22.

Applying the blow-down transformations defined by the local coordinate formulae in (25) yields the map

$$\pi_\varepsilon(r, \theta, R^2, \varepsilon) = \left(R, \theta + \varepsilon^{\alpha-1} \left(\frac{R^2}{\varepsilon^2} + \Omega_0 \right) (1 + \mathcal{O}(R)) + \mathcal{O} \left(\varepsilon^\alpha \ln \frac{1}{\varepsilon} \right) \bmod 1, -\Omega_0 \varepsilon^2 + \mathcal{O} \left(\varepsilon^3 \ln \frac{1}{\varepsilon} \right), \varepsilon \right), \quad (41)$$

for all $\varepsilon \in (0, \varepsilon_0]$ (the limiting value $\varepsilon = 0$ is omitted because the blow-down transformation is only defined for $\varepsilon > 0$). This proves Assertion (a) in Theorem 3.2, since the map π is identified with π_ε after omitting the trivial component $\varepsilon \mapsto \varepsilon$.

It remains to prove the strong contraction property in Assertion (b). This can be done by differentiating the expression for Π . Letting $\mathcal{Q} := \Pi_3 \circ \kappa_{23} \circ \Pi_2 \circ \kappa_{12}$, we obtain

$$\frac{\partial \Pi}{\partial r_1}(r_1, \theta_1, R, \varepsilon_1) = \frac{\partial \mathcal{Q}}{\partial r_1}(\Pi_1(r_1, \theta_1, R, \varepsilon_1)) \frac{\partial \Pi_1}{\partial r_1}(r_1, \theta_1, R, \varepsilon_1),$$

after applying the chain rule. Direct calculations using Lemma 4.1, Propositions 4.16 and 4.22 show that $(\partial \mathcal{Q} / \partial r_1)(\Pi_1(r_1, \theta_1, R, \varepsilon_1))$ is (at worst) algebraically growing in r_1 and ε_1 . Since the second term $(\partial \Pi_1 / \partial r_1)(r_1, \theta_1, R, \varepsilon_1)$ is exponentially small due to the strong contraction in K_1 , recall Proposition 4.11 Assertion (b), it follows that

$$\frac{\partial \Pi}{\partial r_1}(r_1, \theta_1, R, \varepsilon_1) = \mathcal{O} \left(e^{-2\kappa/3\varepsilon_1^3} \right),$$

for a constant $\kappa \in (0, c) \subset (0, 2)$, assuming the constant E bounding ε_1 is sufficiently small. Assertion (b) in Theorem 3.2 follows for all $\varepsilon \in (0, \varepsilon_0]$ with ε_0 sufficiently small after applying the blow-down transformation (in particular $\varepsilon_1 = \varepsilon/R$). \square

Remark 4.25. We recall from the discussion following the proof of Theorem 3.2 that the total number of rotations about the y -axis as solutions traverse the neighbourhood from Δ^{in} up to Δ^{out} can be read off of the θ -component of the image $\pi(r, \theta, R^2)$ or, equivalently, $\pi_\varepsilon(r, \theta, R^2, \varepsilon)$ in equation (41) above. The total number of rotations is given by

$$N_{\text{rot}}(\varepsilon, \alpha) = \lfloor R^2 (\varepsilon^{\alpha-3} + \Omega_0 \varepsilon^{\alpha-1}) (1 + \mathcal{O}(R)) + \mathcal{O}(\varepsilon^\alpha \ln \varepsilon) \rfloor.$$

Recalling Remarks 4.10, 4.17 and 4.24, we see that the $\mathcal{O}(\varepsilon^{\alpha-3})$, $\mathcal{O}(\varepsilon^{\alpha-1})$ and $\mathcal{O}(\varepsilon^\alpha \ln \varepsilon)$ terms correspond to rotations in the regions considered in charts K_1 , K_2 and K_3 respectively.

5 Summary and outlook

GSPT is an established and powerful tool for the analysis of stationary fast-slow systems, particularly when combined with the blow-up method. The corresponding theory for oscillatory fast-slow systems which possess a limit cycle manifold instead of (or in addition to) a critical manifold is less developed, despite the fact that oscillatory systems are common in applications. One reason for this appears to be that the theory for stationary fast-slow systems, notably Fenichel-Tikhonov theory and the blow-up method, depend on quasi-equilibrium properties possessed by stationary but not oscillatory fast-slow systems. The main purpose of this article has been to show that both Fenichel-Tikhonov theory and blow-up method can be applied to study the dynamics of a class of multiple time-scale systems with three or more time-scales, as long as the angular/rotational dynamics are sufficiently slow relative to the radial dynamics. The class of systems considered, namely those in the general form (4), contains a class of systems that are oscillatory with respect to the partial singular limit $\varepsilon_1 > 0$, $\varepsilon_2 \rightarrow 0$, but stationary with respect to the double singular limit $(\varepsilon_1, \varepsilon_2) \rightarrow (0, 0)$. Our analysis showed that Fenichel-Tikhonov theory and the blow-up method can be applied directly to such systems, given the quasi-equilibrium properties of the double singular limit.

More concretely, we focused on the dynamics near a (three time-scale) global singularity corresponding to a regular folded cycle bifurcation in the layer problem. In order to do so we derived a normal form for the three time-scale global singularity near the non-hyperbolic cycle S_0^c , recall Proposition 2.1, and studied the transition map induced by the flow. Our main result is Theorem 3.2, which is stated for the simplified normal form (11), which provides a rigorous characterisation of the asymptotic and strong contraction properties of the flow near S_0^c . The asymptotics for $h_y(r, \theta, \varepsilon)$ (i.e. the parameter drift in the y -component) and the strong contraction property are the same as for the stationary regular fold point studied in [37, 46], and do not depend on the additional parameter α , which determines the relative time-scale of the dynamics in θ and y . The asymptotic estimates for the angular component $h_\theta(r, \theta, \varepsilon)$ do depend on α , and the total number of rotations about the y -axis varies significantly in cases (C1)*, (C1), (C2) and (C3); recall the varying estimates for $N_{\text{rot}}(\varepsilon, \alpha)$ near the end of Section 3. Theorem 3.2 is proved using the blow-up method in Section 4, thereby demonstrating the applicability of geometric blow-up techniques to study global singularities of limit cycle type in suitable classes of three time-scale systems. The proof is somewhat simplified by the fact that the simplified normal form only depends on θ in the higher orders (recall Assumption 3), since in this case, the equation for θ decouples in the leading order desingularized system on the blow-up surface. Given that desingularization is still possible if one considers the ‘full’ normal form (7), however, we also expect the blow-up method to apply in this more general setting; recall Remark 4.5.

The current manuscript provides a precedent for the effectiveness of stationary methods including Fenichel-Tikhonov theory and the blow-up method in oscillatory multiple time-scale systems with at least three time-scales. Since our focus was on the development of a method, simplifying assumptions like Assumption 3 were made so that we could appeal to known results in order to simplify and streamline the ‘classical’ analysis in coordinate charts within the blow-up. New effects and qualitative distinctions between the regular folded cycle singularity and its stationary counterpart may arise if one works directly with the full normal form in Proposition 2.1. Another open question concerns the applicability of the methods developed herein for other global cycle singularities for which there is no direct and lower dimensional analogue in stationary fast-slow systems, e.g. near a non-hyperbolic flip/period-doubling type cycle in three time-scale systems of the form (4). These and other related problems are left for future work.

Acknowledgements

SJ, SVK and CK acknowledge funding from the SFB/TRR 109 Discretization and Geometry in Dynamics grant. SVK also acknowledges funding from the DFG priority program SPP 2298 Theoretical Foundations of Deep Learning as well as the Munich Data Science Institute. CK thanks the VolkswagenStiftung for support via a Lichtenberg Professorship.

References

- [1] O. D. ANOSOVA, *On invariant manifolds in singularly perturbed systems*, Journal of Dynamical and Control Systems, 5 (1999), pp. 501–507.
- [2] ———, *Invariant manifolds in singularly perturbed systems*, Trudy Matematicheskogo Instituta Imeni VA Steklova, 236 (2002), pp. 27–32.
- [3] C. BAESENS, *Slow sweep through a period-doubling cascade: Delayed bifurcations and renormalisation*, Physica D: Nonlinear Phenomena, 53 (1991), pp. 319–375.
- [4] ———, *Gevrey series and dynamic bifurcations for analytic slow-fast mappings*, Nonlinearity, 8 (1995), p. 179.
- [5] E. BASPINAR, D. AVITABILE, AND M. DESROCHES, *Canonical models for torus canards in elliptic bursters*, Chaos: An Interdisciplinary Journal of Nonlinear Science, 31 (2021), p. 063129.
- [6] G. N. BENES, A. M. BARRY, T. J. KAPER, M. A. KRAMER, AND J. BURKE, *An elementary model of torus canards*, Chaos: An Interdisciplinary Journal of Nonlinear Science, 21 (2011), p. 023131.
- [7] R. BERTRAM, M. J. BUTTE, T. KIEMEL, AND A. SHERMAN, *Topological and phenomenological classification of bursting oscillations*, Bulletin of Mathematical Biology, 57 (1995), pp. 413–439.
- [8] P. CARDIN, P. DA SILVA, AND M. TEIXEIRA, *Three time scale singular perturbation problems and nonsmooth dynamical systems*, Quarterly of Applied Mathematics, 72 (2014), pp. 673–687.
- [9] P. T. CARDIN AND M. A. TEIXEIRA, *Fenichel theory for multiple time scale singular perturbation problems*, SIAM Journal on Applied Dynamical Systems, 16 (2017), pp. 1425–1452.
- [10] M. L. CARTWRIGHT AND J. E. LITTLEWOOD, *On non-linear differential equations of the second order II*, Annals of Mathematics, (1947), pp. 472–492.
- [11] P. DE MAESSCHALCK, E. KUTAFINA, AND N. POPOVIĆ, *Three time-scales in an extended Bonhoeffer–van der Pol oscillator*, Journal of Dynamics and Differential Equations, 26 (2014), pp. 955–987.
- [12] M. DESROCHES, J. BURKE, T. J. KAPER, AND M. A. KRAMER, *Canards of mixed type in a neural burster*, Physical Review E, 85 (2012), p. 021920.
- [13] M. DESROCHES AND V. KIRK, *Spike-adding in a canonical three-time-scale model: Superslow explosion and folded-saddle canards*, SIAM Journal on Applied Dynamical Systems, 17 (2018), pp. 1989–2017.
- [14] F. DUMORTIER AND R. ROUSSARIE, *Canard cycles and center manifolds*, no. 577 in Memoirs of the American Mathematical Society, American Mathematical Society, 1996.
- [15] B. ERMENTROUT AND D. H. TERMAN, *Mathematical foundations of neuroscience*, vol. 35, Springer, 2010.
- [16] N. FENICHEL, *Geometric singular perturbation theory for ordinary differential equations*, Journal of Differential Equations, 31 (1979), pp. 53–98.
- [17] A. FRUCHARD AND R. SCHÄPFKE, *A survey of some results on overstability and bifurcation delay*, Discrete & Continuous Dynamical Systems-S, 2 (2009), p. 931.

- [18] J. GRASMAN, *Asymptotic methods for relaxation oscillations and applications*, Springer-Verlag, 1987.
- [19] J. GUCKENHEIMER, *Towards a global theory of singularly perturbed dynamical systems*, in *Nonlinear Dynamical Systems and Chaos*, Springer, 1996, pp. 213–225.
- [20] J. GUCKENHEIMER, J. H. TIEN, AND A. R. WILLMS, *Bifurcations in the fast dynamics of neurons: implications for bursting*, in *Bursting: The Genesis of Rhythm in the Nervous System*, World Scientific, 2005, pp. 89–122.
- [21] Y. ILYASHENKO, *Embedding theorems for local maps, slow-fast systems and bifurcation from Morse-Smale to Smale-Williams*, *Translations of the American Mathematical Society-Series 2*, 180 (1997), pp. 127–140.
- [22] Y. ILYASHENKO, *Selected topics in differential equations with real and complex time*, *Normal Forms, Bifurcations and Finiteness Problems in Differential Equations*, in: *NATO Sci. Ser. II Math. Phys. Chem*, 137 (2004), pp. 317–354.
- [23] J. JALICS, M. KRUPA, AND H. G. ROTSTEIN, *Mixed-mode oscillations in a three time-scale system of ODEs motivated by a neuronal model*, *Dynamical Systems*, 25 (2010), pp. 445–482.
- [24] H. JARDÓN-KOJAKHMETOV AND C. KUEHN, *A survey on the blow-up method for fast-slow systems*, arXiv preprint arXiv:1901.01402, (2019).
- [25] S. JELBART AND C. KUEHN, *Discrete geometric singular perturbation theory*, arXiv preprint arXiv:2201.06996, (2022).
- [26] C. K. JONES, *Geometric singular perturbation theory*, in *Dynamical systems*, vol. 1609 of *Lecture Notes in Mathematics*, Springer, 1995, pp. 44–118.
- [27] P. KAKLAMANOS AND N. POPOVIĆ, *Complex oscillatory dynamics in a three-timescale El Niño southern oscillation model*, arXiv preprint arXiv:2207.03230, (2022).
- [28] P. KAKLAMANOS, N. POPOVIĆ, AND K. U. KRISTIANSEN, *Bifurcations of mixed-mode oscillations in three-timescale systems: An extended prototypical example*, *Chaos: An Interdisciplinary Journal of Nonlinear Science*, 32 (2022), p. 013108.
- [29] ———, *Geometric singular perturbation analysis of the multiple-timescale Hodgkin-Huxley equations*, arXiv preprint arXiv:2203.02948, (2022).
- [30] I. KOSIUK AND P. SZMOLYAN, *Geometric singular perturbation analysis of an Autocatalator model*, *Discrete and Continuous Dynamical Systems*, 2 (2009), pp. 783–806.
- [31] ———, *Scaling in singular perturbation problems: Blowing up a relaxation oscillator*, *SIAM Journal on Applied Dynamical Systems*, 10 (2011), pp. 1307–1343.
- [32] ———, *Geometric analysis of the Goldbeter minimal model for the embryonic cell cycle*, *Journal of Mathematical Biology*, 72 (2016), pp. 1337–1368.
- [33] M. A. KRAMER, R. D. TRAUB, AND N. J. KOPELL, *New dynamics in cerebellar purkinje cells: Torus canards*, *Physical Review Letters*, 101 (2008), p. 068103.
- [34] K. U. KRISTIANSEN AND P. SZMOLYAN, *Relaxation oscillations in substrate-depletion oscillators close to the nonsmooth limit*, *Nonlinearity*, 34 (2021), p. 1030.
- [35] N. KRUFF AND S. WALCHER, *Coordinate-independent singular perturbation reduction for systems with three time scales*, *Mathematical Biosciences and Engineering*, 16 (2019), pp. 5062–5091.
- [36] M. KRUPA, N. POPOVIĆ, AND N. KOPELL, *Mixed-mode oscillations in three time-scale systems: A prototypical example*, *SIAM Journal on Applied Dynamical Systems*, 7 (2008), pp. 361–420.

- [37] M. KRUPA AND P. SZMOLYAN, *Extending geometric singular perturbation theory to nonhyperbolic points—fold and canard points in two dimensions*, SIAM Journal on Mathematical Analysis, 33 (2001), pp. 286–314.
- [38] ———, *Extending slow manifolds near transcritical and pitchfork singularities*, Nonlinearity, 14 (2001), p. 1473.
- [39] ———, *Relaxation oscillation and canard explosion*, Journal of Differential Equations, 174 (2001), pp. 312–368.
- [40] C. KUEHN, *Multiple time scale dynamics*, vol. 191 of Applied Mathematical Sciences, Springer, 2015.
- [41] C. KUEHN, N. BERGLUND, C. BICK, M. ENGEL, T. HURTH, A. IUORIO, AND C. SORESINA, *A general view on double limits in differential equations*, Physica D: Nonlinear Phenomena, 431 (2022), p. 133105.
- [42] C. KUEHN AND P. SZMOLYAN, *Multiscale geometry of the Olsen model and non-classical relaxation oscillations*, Journal of Nonlinear Science, 25 (2015), pp. 583–629.
- [43] Y. A. KUZNETSOV, *Elements of applied bifurcation theory*, vol. 112 of Applied Mathematical Sciences, Springer Science & Business Media, 2013.
- [44] B. LETSON, J. E. RUBIN, AND T. VO, *Analysis of interacting local oscillation mechanisms in three-timescale systems*, SIAM Journal on Applied Mathematics, 77 (2017), pp. 1020–1046.
- [45] I. LIZARRAGA, B. RINK, AND M. WECHSELBERGER, *Multiple timescales and the parametrisation method in geometric singular perturbation theory*, Nonlinearity, 34 (2021), p. 4163.
- [46] E. MISHCHENKO AND N. ROZOV, KH, *Differential equations with small parameters and relaxation oscillations*, Nauka, Moscow. (transl.: Plenum Press, New York, 1980), 1975.
- [47] P. NAN, Y. WANG, V. KIRK, AND J. E. RUBIN, *Understanding and distinguishing three-time-scale oscillations: Case study in a coupled Morris–Lecar system*, SIAM Journal on Applied Dynamical Systems, 14 (2015), pp. 1518–1557.
- [48] K. NIPP AND D. STOFFER, *Invariant manifolds in discrete and continuous dynamical systems*, vol. 21 of EMS Tracts in Mathematics, European Mathematical Society, 2013.
- [49] K. NIPP, D. STOFFER, AND P. SZMOLYAN, *Graph transform and blow-up in singular perturbations*, in AIP Conference Proceedings, American Institute of Physics, 2009, pp. 861–868.
- [50] L. S. PONTRYAGIN AND L. V. RODYGIN, *Approximate solution of a system of ordinary differential equations involving a small parameter in the derivatives*, in Doklady Akademii Nauk, vol. 131, Russian Academy of Sciences, 1960, pp. 255–258.
- [51] J. RINZEL, *A formal classification of bursting mechanisms in excitable systems*, in Mathematical Topics in Population Biology, Morphogenesis and Neurosciences, Springer, 1987, pp. 267–281.
- [52] K.-L. ROBERTS, J. E. RUBIN, AND M. WECHSELBERGER, *Averaging, folded singularities, and torus canards: Explaining transitions between bursting and spiking in a coupled neuron model*, SIAM Journal on Applied Dynamical Systems, 14 (2015), pp. 1808–1844.
- [53] P. SZMOLYAN AND M. WECHSELBERGER, *Canards in \mathbb{R}^3* , Journal of Differential Equations, 177 (2001), pp. 419–453.
- [54] ———, *Relaxation oscillations in \mathbb{R}^3* , Journal of Differential Equations, 200 (2004), pp. 69–104.
- [55] A. N. TIKHONOV, *Systems of differential equations containing small parameters in the derivatives*, Matematicheskii Sbornik, 73 (1952), pp. 575–586.
- [56] T. VO, *Generic torus canards*, Physica D: Nonlinear Phenomena, 356 (2017), pp. 37–64.

- [57] M. WECHSELBERGER, *Geometric singular perturbation theory beyond the standard form*, in *Frontiers in Applied Dynamical Systems: Reviews and Tutorials*, Springer International Publishing, 2020.
- [58] S. WIGGINS, *Normally hyperbolic invariant manifolds in dynamical systems*, vol. 105, Springer Science & Business Media, 1994.